New Device Structures for Organic Photovoltaics Using Transfer Printing

by

Husna Anwar

Submitted to the Department of Physics
in partial fulfillment of the requirements for the degree of

Bachelor of Arts

at

MOUNT HOLYOKE COLLEGE

May 2015

Author .....
Department of Physics
May 17, 2015

Certified by .....
Alexi C. Arango
Assistant Professor
Thesis Supervisor

Accepted by .....
Mark Peterson
Chair, Department of Physics

New Device Structures for Organic Photovoltaics Using Transfer Printing

by

Husna Anwar

Submitted to the Department of Physics
on May 17, 2015, in partial fulfillment of the
requirements for the degree of
Bachelor of Arts

Abstract

Organic photovoltaics provide an inexpensive and lightweight alternative to conventional silicon solar panels. However, low power conversion efficiencies, mainly due to low open-circuit voltage (V_{OC}) prevent them from competing with silicon cells commercially. Poly (3-hexylthiophene-2, 5-diyl) (P3HT) is a polythiophene derivative that is a popular electron-donor material used in organic solar cells. However, the highest V_{OC} reported for well-performing P3HT/fullerene solar cells is around 0.80 V. This is much lower than would be expected for a donor with a 1.8eV bandgap such as P3HT, and indicates over a 44% loss compared with the theoretical limit. The most popular morphology for the active layer in OPVs currently involves a blend deposition method in which acceptor and donor materials are processed together in solution before deposition. While this device architecture allows for increased interfacial surface area between the acceptor and donor, it also increases leakage and recombination at the interface leading to reduced V_{OC} and shunt resistance. We propose a planar device structure that could allow us to suppress interfacial recombination. This device structure could be scaled-up for quick, mass production through roll-to-roll processing. Using print deposition, we have fabricated an unconventional structure consisting of pristine layers of P3HT as an electron donor and [6,6]-penyl-C61-butyric-acid-methyl-ester (PCBM) as the electron acceptor to form a planar cell. Our deposition method also employs print deposition to place thin Lead(II)Sulphide quantum dot (PbS QD) films and PCBM electron acceptor on top of our spin-cast P3HT layer. We investigate electron-hole pair dissociation at the donor-acceptor interface by inserting an additional film between the donor and acceptor layers and observing the impact on V_{OC}. We employ the small molecule, Tris(8-hydroxyquinolinato)aluminium (Alq3), and see an improvement in V_{OC}. We propose that the proper material, when placed at the interface, suppresses non-geminate recombination and can increase V_{BI}. We have extend our investigation to vapor deposited materials, 2,2',7,7'-Tetrakis-(N,N-di-4-methoxyphenylamino)-9,9'-spirobifluorene (Spiro-OMeTAD) and buckminsterfullerene (C60), and document the observed changes in V_{BI}.

Thesis Supervisor: Alexi C. Arango
Title: Assistant Professor

Acknowledgments

First, I would like to thank my advisor, Professor Alexi Arango. His inspirational ideas and undying patience with my incessant questions defined my undergraduate education. I would not be half the researcher I am today without his mentorship.

Next, I must express my gratitude to Professor Maria Gomez for serving on my committee and showing me the beauty in computational chemistry models. Professor Spencer Smith for also serving on my committee and being an incredible teacher and an inspiration for how I hope to live my life.

I must also thank my lab mates. Specifically, Kanchi, for being my partner in crime through many long nights and a constant source of support, this thesis would not exist without her. Phoebe, for showing me how to grow my first cells and being a great role model. Maggie, for her extensive knowledge, sound advice and much-needed reassurance. And Shola, for always making me feel better about my stupid mistakes and keeping me entertained.

This work would also not have been possible without the overwhelming love and support I received from my friends, old and new. Abbas and the Tunafish for always being pleasantly surprised at my achievements. My roommates, Claire, Anna Lee and Huda for being my sisters away from home. Lastly, Madi, Karla, Karishma, Allie, Waad, Pheona, Colbie, K, Kay and the physics clan, who managed to make homework sessions at 3 am feel like a party.

I would like to thank my professors, mentors and idols: Professor Juan Burciaga for his sharp wit and endless supply of interesting facts. Professor Kathy Aidala for her honesty, dedication to helping international students and women in science and her readiness to try and troubleshoot practically any problem her students are facing. Finally, Professor Dylan Shepardson, my adoptive advisor in all matters from courses to paper dinosaurs and how to keep sane. He is the reason I persevered with research and physics.

Lastly, I must acknowledge my family and many siblings individually. My parents, Arjumand and Anwar, for dedicating their lives to the education and growth of their

abundant brood. Marium, for her infectious enthusiasm for learning. Ainy, for always being frank and direct with her advice. Ramsha, thank you for always reminding me that phoneyness is a crime. Sara, for always being irrationally overexcited about my projects and inspiring me to feel the same way. Rafay, for supporting me in every way possible — emotionally, mentally and financially. Finally, Zahra, for being my rock and guide from the minute I set foot in this country — this thesis is dedicated to you.

Contents

List of Figures

Chapter 1

Introduction

Collecting the suns abundant energy through photoconversion using solar panels offers a viable, long-term solution for a sustainable future. As carbon dioxide levels rise and oil reserves run low, there is a growing need for alternative fuel sources.

In 2013, only 6% of the United States energy came from renewable sources, of which a mere 0.23% was generated through solar power [9]. The low adoption of solar energy around the world can be in part attributed to the fact that commercial silicon solar panels are bulky, expensive and come with a complicated and lengthy manufacturing process. Organic photovoltaics (OPVs), consisting of organic materials, provide an alternative to conventional silicon solar panels. OPVs are inexpensive, easy to produce, lightweight and flexible. However, low power conversion efficiencies prevent OPVs from competing with silicon cells commercially. One of the most well-studied, but least understood, areas of OPVs is the mechanism in which voltage is generated in these devices.

In the next section, we present a high-energy demand city in a developing country as a case study for the need for cheap, easily accessible power generation methods.

Finally, we propose a new device structure and fabrication method that would allow us to push device performance above the current 12% [30] highest efficiency OPV device today.

1.1 Karachi: A Case Study

Karachi is large coastal city in south of Pakistan with a population of over 9 million people. The city is the industrial hub of the country, demanding over 60 million kiloWatt-hours (kWh) of energy every day. This includes commercial as well as residential users that amount to over 2 million (as counted by electricity collection meters).

The average cost of energy in this city is Rs.15 ($0.15) per kWh, amounting to a total monthly bill of about $60 for the average household. Considering 60.3% of people in Pakistan live on under $2 a day, spending $60 on electricity every month is the average person's entire salary being spent on electricity alone - let an extraneous expense on top of paying for education, medicine or even food, water and housing [2].

Due to the high cost of power and low incomes, there is a high amount of energy theft. The Karachi Electricity Supply Company or K-Electric reports an average loss of 23% to energy theft and grid losses [4], with this number rising to 40% in high-theft areas.

The company has a generation capacity of 50 million kWh per day, of which approximately 45% is self-generated from petroleum and natural gas. According to Rashid Hussain, the deputy director of the company, the rest of the energy is purchased from the National Grid and Private Power Producers. The remaining 15% of the 60 mkWh daily demand is met by "load-shedding" at high-loss areas during peak demand hours. Load-shedding is when energy companies switch their generators off during peak demand in order to meet demand at other times. The harsh reality of these circumstances is that a city with an average yearly temperature of 89.1 F [3] is left with no cooling facilities at hours of peak demand. While most hospitals, commercial centers and high income households are able to afford diesel generators to privately generate power, lower income households and lower funded facilities (including schools) are not as fortunate.

Karachi receives about 19.5 mega joules per square meter day (MJ/m^2d) of solar isolation with an annual total of 7000 MJ/m^2. The influx of global solar radiation is

(a)

(b)

Figure 1-1: (a) The commercial center of Karachi. The city consumes 25 million kWh at peak consumption which levels out to an average of 60 million kWh over the course of the day. (b) Transformers often burn out under the load of all the illegal connections that find their way onto the pylons.

very consistent, with a variation of only 22.8% in the last 27 years [6]. For the city's 60 million kWh daily demand to be met, a mere 2592 MJ/m^2 of that 7000 MJ/m^2 solar insolation needs to be harvested.

The city sprawls over 3,527 km^2. If only 0.5% of the city's land mass was to be covered with 15% efficient solar panels, the panels would generate enough to meet the entire city's energy demand.

Many industrial cities in developing countries have similar energy needs and solar insolation. For inaccessible and underdeveloped areas, scalability, ease of manufacturing and installation and decentralized power stations are all necessities for power generation methods. Lightweight, flexible modules can be just as easily installed on a thatched roof as on a factory. This technology can better millions of lives - in the context of Karachi's case study, that is over 9 million in one city alone.

1.2 Proposed Device Architecture

As mentioned earlier, low power conversion efficiencies are the prime reason that organic photovoltaics have not yet replaced silicon panels. The transfer printing method we present in this thesis allows us to create device architectures that could boost V_{OC}, and hence the efficiency, of these devices.

In this section we briefly discuss the evolution of OPV device architecture and explain how our proposed structure may allow for higher device performance. Finally we provide a summary of the work presented in this thesis.

1.2.1 History of OPVs

The discovery of conductive polymers in 1977 won Heeger, McDiarmid and Shirakawa the Noble Prize and heralded a new era for technology ([32]). Devices were no longer restricted by the labor intensive fabrication and rigid properties of glass and silicon based displays. Smart phones became smaller and televisions lighter. Solar energy jumped on the bandwagon with the second generation of photovoltaics – the flexible copper indium gallium selenide (CIGS) panels. The scientists behind these panels

however, compromised efficiency in order to create lightweight, flexible and cheap solar.

The next generation of solar energy is OPVs. Devices have evolved from heavy, but efficient, silicon-based panels to flexible but CIGS panels that exhibit much lower efficiencies. Researchers working on the third generation of photovoltaics aims to raise efficiency while maintaining flexibility and ease of fabrication by using organic materials such as dyes, fullerenes and polymers [29].

In 1986, Tang fabricated the first bilayer OPV using copper phthalocyanine and a perylene tetracarboxylic derivative [37]. His cell generated an efficiency of 1% and revolutionized the field. So far, cells had consisted only of an organic photovoltaic material placed between asymmetric metal electrodes as a Schottky device. Tang was the first to introduce the donor-acceptor structure. He also pointed out the necessary role of the interface for charge separation into free carriers.

Common Device Structures

Though Tang's cell vastly improved device performance, the bilayer device still demonstrated low efficiency due to short exciton diffusion lengths (§2.1). A number of device architectures meant to target this source of loss developed over the next few decades, the most popular of which was the bulk heterojunction (BHJ). Presented by Heeger simultaneously with Friend and Holmes, this device architecture sought to negate the effect of excitons recombining before reaching the interface. They achieved this by simply increasing the interface by intermixing the donor and acceptor in solution before fabrication (see Fig. 1-2). These devices, however, suffer from their own set of issues including charge trapping and interfacial recombination (§2.2).

Device architecture evolved from this point to include interfacial layers at the electrodes to prevent exciton quenching and charge leakage at the organic-metal interface. Trilayer p-i-n cells are comprised of an absorbing blend layer sandwiched between a pair of wide-bandgap donor and acceptor layers. The advantage to this architecture is that each layer can be optimized independently of others. However, they require very meticulous energy alignment between the three materials.

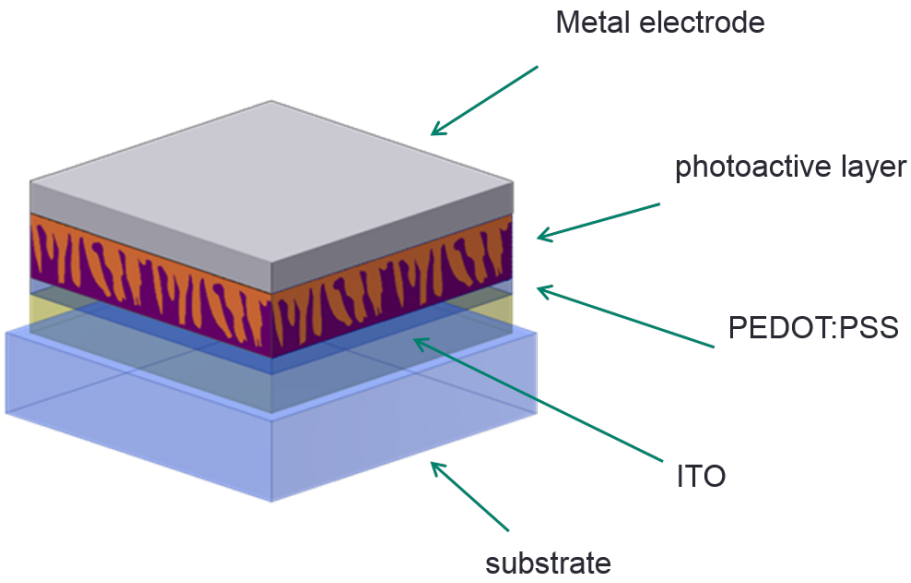

Figure 1-2: Structure of a bulk heterojunction device. In this work we use silver as our cathode material and P3HT:PCBM as our active layer.

Dye sensitized solar cells have similar structures that employ using a thin, highly absorbing dye to boost photogeneration in the cell. Recently, perovskite solar cells have gained popularity almost overnight. Layered organicinorganic perovskites have been successfully used for flexible, light-emitting devices, as well as field- effect transistors, and are now crossing over to the world of OPVs generating efficiencies of almost 18% efficient devices [12] [27].

1.3 Our Theory and Proposed Architecture

BHJ devices tend to have intermixed, disordered structures. Extensive phase segregation leads to large domains of material that can result in bad electrode contacts and hence charge leakage at the contacts because of exciton quenching at the organic-metal interface [16]. The need to prevent this loss at the electrode interface first brought about the use of interfacial layers at the contacts.

One of the most commonly used contact interfacial materials is PEDOT:PSS which is what we use in our device structure at the ITO contact. 2,9-dimethyl-4,7-diphenyl-1,10- phenanthroline (BCP) is another interfacial material that is commonly

used in OLEDs and helps electron injection. BCP's charge injection properties make it ideal for use as an interfacial layer at the cathode. Tris(8-hydroxyquinoline) aluminum (Alq3) is another such material that evolved from its use in OLEDs to OPVs. In this work we make use of its wide-bandgap and electron injecting properties by placing it as an interfacial layer at the donor-acceptor interface to suppress interfacial recombination.

Alq3 was easy to deposit as it can be vapor deposited at the interface. Solution-processable materials however, are more tricky. In the next section we explain why it very challenging to deposit multiple layers of solution-processable materials and present a fabrication method that allows us to overcome the issue of multiple layer wet deposition.

1.3.1 Transfer Printing

As Chen et al (2008) explain, transfer printing using a silicon elastomer stamp negates the problem of solvent orthogonality in fabricating polymer multilayers [14]. The advantage of this method is that it does not require any chemical modification of the materials to be deposited. It is near impossible to print consecutive layers of solution-processed materials because each additional layer deposited will damage or remove the previously deposited layer by introducing fresh solvent to the system. The only way to achieve multiple layers of pristine material is to dissolve each material in a separate solvent that will not mix with the previous layer. This requirement only adds another layer of complication to the process of solvent processing. As we speak demonstrate in the Methods section, choice of solvent is imperative to achieving good molecular arrangement in each solution-processed material. Chloroform, for example, was found to be the ideal solvent for both the donor and acceptor material used in this work. The only way to create a pristine bilayer structure using conventional spin-casting deposition methods is to change the solvent used for one of the two materials. The transfer printing process used in this work allows the material to completely dry on a squishy poly(dimethylsiloxane) (PDMS) stamp before transferring it to the substrate. Allowing the solvent to completely evaporate before transfer printing makes this a

dry-deposition process. Hence the same solvent can be used for multiple materials and layers can be printed in quick succession.

Denegaar et al propose using a soft stamp for micro-printing. They demonstrate printing patterned layers by using nanostructured PDMS to print on a substrate coated with a fine layer of glycerol.

Yim et al (2008) employed an interesting combination of a sacrificial layer and used a PDMS stamp to pick a pre-deposited layer of polymeric material up off of a silicon wafer. The group then stamped the material onto a flexible substrate, supporting the claim that this deposition method is ideal for quick roll-to-roll processing [42]. In 2009, Huang et al showed that pre-wetting the PDMS reduces surface tension, allowing the printed material to coat the PDMS more uniformly. They were able to achieve efficiencies of 3.2% for their direct P3HT:PCBM structures [18].

All these methods, however, were optimized for polymers. As we explain later, polymers form cross-linked chains and are hence easier to transfer. In this work, our goal is to print all materials - pristine [6,6]-penyl-C61-butyric-acid-methyl-ester (PCBM) in particular - which has never been transfer printed before. PCBM presents a unique set of challenges due to its tendency to aggregate and form large domains.

1.3.2 Device Concept: The Importance of the Interface

It is commonly accepted, as we explain in the next chapter, that the maximum open-circuit voltage (V_{OC}) demonstrated by a device is limited by the difference between the highest occupied molecular orbital (HOMO) level of the donor and the lowest unoccupied molecular orbital (LUMO) level of the acceptor, or what we will refer to as the interfacial bandgap. Nelson et al made the claim that, if we are able to suppress interfacial recombination, the efficiency of a donor-acceptor pairing will no longer be limited by the interfacial bandgap, but instead by the optical bandgap of the two [25].

Maurano et al use a computational model to compare four different polymers in blend devices and prove that V_{OC} depends on bimolecular recombination [24]. They demonstrated that V_{OC} depends on the lifetimes of charge carriers within the BHJ

device structure. They later used this claim to address why BHJs cannot achieve the theoretical limit that their optical bandgaps proposed. Maurano et al make the simplifying assumption that V_{OC} is when the flux of charge photogeneration (or, more specifically, the flux of generation of dissociated charges) is equal and opposite to the flux of recombination of these dissociated charges. They then measure charge carrier densities and decay dynamics as a function of light intensity which allows them to see the effect of charge trapping and calculate the variation in V_{OC} for the four polymers.

Shuttle et al have also proven the dependence of V_{OC} on bimolecular recombination using transient absorption on both P3HT:PCBM devices and films. They conclude that "minimization of such bimolecular losses is likely to be essential to improve the voltage output, and therefore power conversion efficiency, of P3HT:PCBM solar cells." [33].

The consensus appears to be that finding a way to suppress interfacial recombination is necessary to achieving higher open-circuit voltage and efficiency. Tada et al demonstrate this by using a very different fabrication technique from what we propose but with essentially the same device concept. They employ a film-transfer method in which they grow two devices, and then join them together using a sacrificial PSS layer that can be dissolved in water. Next, they modified each film with a surface-segregated monolayer to tune the strength and direction of the surface dipole moment. Following this, they use these dipole moments to tune the energy levels at the interface and are hence able to tune the the V_{OC} between 0.3 and 0.95 V.

Even though Tada et al's concept is very different from ours, they conclude that "even if the same combination of bulk materials is used, the interfacial properties drastically alter the performance of organic photovoltaic device [36]. We aim to achieve similar results by modifying the interface using the more intrusive, direct method of introducing a thin layer of material at the interface in the form of an interstitial layer.

This device concept was directly demonstrated for the first time by Nie et al earlier this year (2015). They placed a few nanometers of lithium fluoride as a "spacer" layer between a 1'q and C60 in a bilayer cell and were able to improve photocurrent by

$200 - 350\%$ and efficiency 2-5 times [26]. They also demonstrated similar changes in efficiency using a terthiophene-derivative (O3) and the metal organic complex (bis(1-phenylisoquinoline)-(acetylacetonate) iridium (III) (Irpiq).

Though Nie et al's result was published after we had demonstrated proof of concept for our device architecture using an Alq3 interstitial layer (described in the results section), their findings serve to confirm our results and to solidify the device concept.

1.4 Conclusion

In the following chapter we describe the basic device physics of an OPV device and delve deeper into specific aspects of our device concept. Next we lay out the methods we used to fabricate our devices, including a new transfer printing technique to create pristine bilayer devices. We also explain our choice of materials.

Finally we present our data including a record high J_{SC} device comprised of lead(II)Sulphide quantum dots and a device with an Alq3 interfacial layer that demonstrates unprecedentedly high V_{BI}. We also present the results of our ongoing experimentation and discuss the implications of our findings. We conclude that, while this document describes a work in progress, there is enough data to prove our device concept. We are also confident that, with the exception of complications with fabrication, we are very close to creating a novel device that could break the current cap on OPV efficiency.

Chapter 2

Device Physics

Almost all organic and dye-sensitized solar cells are what are commonly known as excitonic solar cells. This implies that, instead of individual electron and hole charge carriers, these cells function through the generation and dissociation of coulombically bound electron-hole pairs called excitons (Fig. 2-1).

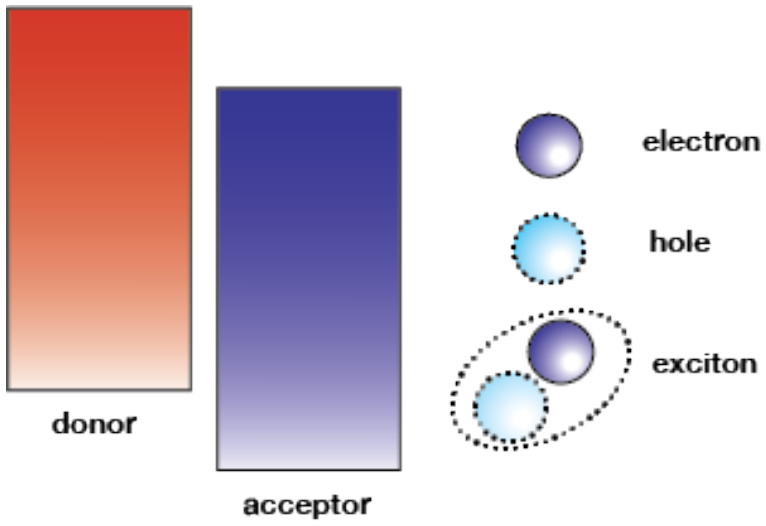

Figure 2-1: Photoexcitation can take place in either the donor or the acceptor material to form a bound electron-hole pair called an exciton.

It is important to remember that unlike amorphous and crystalline silicon devices, OPVs comprise of polymers and other non-crystalline organic materials. This structural difference alone means that the operating mechanism for OPVs, while similar

in theory, is fundamentally different from that of conventional silicon PV. It not only changes the way we interpret their performance, but also creates a whole new set of parameters that limit device behavior.

This chapter will explain how organic solar cells generate current and voltage under illumination and describe how the bulk heterojunction differs from the planar heterojunction cell (§2.1). It will also describe how current-voltage characteristics the cell exhibits are similar to a light-detecting diode (§2.3). Finally it will discuss the factors limiting voltage output and how our proposed device structure might affect this mechanism.

2.1 How do Organic OPVs Function?

The photophysical differences between inorganic photovoltaics and organic photovoltaics stem from their fundamentally different material structure, which we will talk more about in the next chapter. This is also one of the main reasons that the efficiency of OPVs is so low in comparison to that of conventional PV.

In semiconductors like silicon, the crystalline structure allows for much better charge generation and propagation. The lattice creates a pathway of sorts for charge to percolate. At the same time it shields holes and electrons from each other energetically, suppressing recombination and allowing electrons and holes to be generated easily.

In semiconductors such as the ones used in this work, absorption of a photon does not directly result in the production of an electron and a hole. Instead, photoexcitation generates excitons that are electrically neutral and have a binding energy on the order of 0.5 eV [11]. This large binding energy in organic materials is due to the lack of lattice screening together with their lower dielectric constants and the presence of increased trap states [15]]. Before a current can be generated, the exciton must dissociate into its oppositely charged components. As we explain next, this is what makes the donor-acceptor interface integral to the charge generation process.

2.2 Charge Generation Mechanism

There are three main processes through which photocurrent is generated in organic materials. First, the exciton is generated through the absorption of a photon as shown in Fig. 2-2a - this is process can happen in the donor or the acceptor material but usually the donor is chosen to be the absorber. The exciton diffuses through the material and reaches the interface where it forms the charge transfer (CT) state (Fig. 2-2b). In the CT state, the hole and electron are still bound across the interface, with the hole occupying the HOMO level of the donor molecules and the electron at the LUMO level of the acceptor molecules. Through charge separation, the exciton dissociates into a free electron and hole (Fig. 2-2c). Finally the charged particles are extracted through the electrode.

While these charge generation processes are taking place, there are also competing charge and exciton quenching processes occurring. As also shown in Fig. 2-2b, excitons tend to relax into the ground state as they diffuse through the materials and encounter traps, making thickness optimization imperative to good efficiency.

The second greatest loss of efficiency is during the transition from the CT state to the charge-separated state, shown in Fig. 2-2c. The CT state can either dissociate into the CS state, or it can recombine across the interface CT state recombination is the form of recombination this work aims to address. In order to achieve better efficiency, the rate at which the CT and CS states are generated must be maximized while the rates of exciton and CT state recombination must be suppressed.

2.2.1 Dark Current and Photocurrent

Two forms of currents arise when an electron-deficient and an electron-rich semiconductor are put into contact with each other. The drift current is the random motion of electrons due to an electric field, while diffusion current is the movement of charge from higher to lower concentration. The net current is the sum of these two currents.

In a bilayer OPV device, the actual photocurrent depends on a number of other factors including the chemical potential of the material and the intensity of the in-

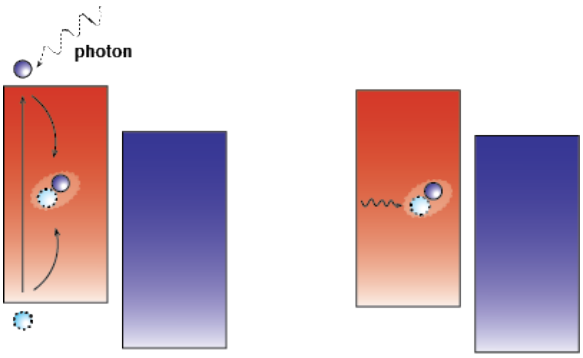

(a) When a photon is incident on the materials, an exciton is generated (left). It is a neutral particle that diffuses randomly through the materials to reach the interface between them (right).

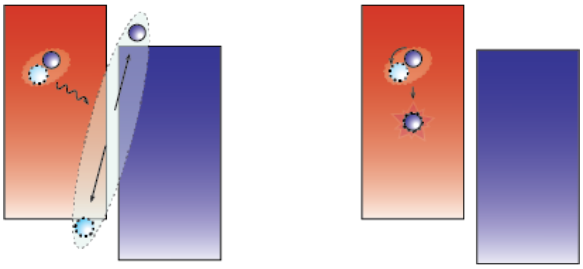

(b) The exciton can either dissociate to form the charge transfer (CT) state (left) or it can recombine before it reaches the interface and release energy (right).

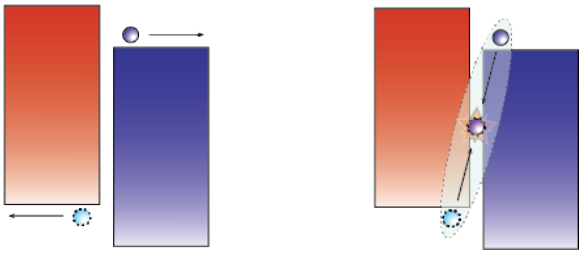

(c) The CT state then separates into free charge carriers (left) or recombines across the interface (right).

Figure 2-2: The charge generation and extraction process in an excitonic solar cell is shown here. For optimal efficiency, the rate of exciton generation and dissociation to the CT state must be greater than the rate of exciton recombination as shown in (b). In (c), the rate of charge separation and extraction through the electrodes must be greater than CT state recombination at the interface.

cident light. The photocurrent is the cumulative effect of hole and electron diffusion and drift when the device is under illumination.

As we saw earlier, excitons form the charge transfer state at the interface. Once they are able to separate, there is a pile up of carriers at the interface as they are unable to recombine across the interface. For instance, in a simple polymer donor-fullerene acceptor device, electrons can move from the polymer to the acceptor. However, there is a large energy barrier (formed by the HOMO-LUMO offset between the two materials) that prevents movement in the opposite direction. This pile-up of charges at the interface creates a carrier concentration gradient that causes charges to diffuse in opposite directions towards the electrodes. In addition, an internal electric-field due to an electrode work function offset will push more charges to the electrodes, ie, setting up a drift current. The photocurrent is due to the overall absorbed photon flux from the sun and so depends on the absorption of the materials used.

Hence, in order to improve photocurrent and possibly even V_{OC}, the charge generation and separation steps must be optimized. We will talk more about how the rates of these different processes need to be complimentary to each other.

If you attach the solar cell to a load, this charge buildup causes a potential difference to develop within the cell. The current set up by this difference is what is called the dark current (J_{dark}) and is a function of the voltage. When we talk about the current-voltage characteristics of the cell, we are talking about the difference between the sum of the dark current and the short circuit photocurrent (J_{SC}). Simply put, the dark current is the current that flows through the device when a bias is applied (or a load is attached) in the dark, so the device is not producing any current or voltage through the photovoltaic effect.

$$J(V) = J_{dark}(V) - J_{SC}$$

Since the two currents oppose each other, we want the dark current to be as low as possible and the photocurrent to be high.

In the dark, a solar cell is simply a diode and behaves similarly to any p-n junction

diode, with a turn-on voltage in forward bias. Light has the effect of shifting the IV curve down into the fourth quadrant where power can be extracted from the diode [6]. The efficiency of a solar cell depends on both open-circuit voltage (V_{OC}) and short-circuit current (J_{SC}) and their ratio with the maximum voltage and maximum current the cell can produce. When a bias is applied across an illuminated cell, V_{OC} is the voltage generated only by the photocurrent J_{SC} is the current produced by the cell under illumination. The greater the J_{SC}, the more the IV curve will be shifted down into the fourth quadrant.

2.3 Open-Circuit Voltage Origins and Limitations

When you create a break in the external circuit - remove the load to create infinite resistance between the contacts - the potential difference is at it's maximum and is called the open-circuit voltage (V_{OC}). This is the same as the point when the dark current and the photocurrent are equal and opposite and so cancel each other out.

It is believed that V_{OC} is directly tied to the offset in the LUMO level of the donor and the HOMO level of the acceptor material [?Dennler2008]. However, recently, many other factors have been found to influence V_{OC}. Nelson et al for example claims that the interfacial bandgap only becomes a limitation when there is high interfacial recombination [25]. They claim that, if recombination at the interface is low enough, the dependence of the V_{OC} increases from the interfacial gap to the actual optical bandgap of the materials.

Parasitic resistances also play a role in limiting V_{OC}. While high series resistance has no effect on V_{OC}, it can lower the J_{SC} and the fill factor of the device. Low shunt resistance however, does lower both V_{OC} and J_{SC}. This is because shunt resistance arrises from leakage of current through the cell, around the edges of the device and between contacts of different polarity [1].

2.3.1 Built-in Voltage vs Open-Circuit Voltage

It is important to make a distinction between open-circuit voltage (V_{OC}) and what we refer to as built-in voltage (V_{BI}). While they are both measures of the device's voltage output under illumination, they are contingent on a separate set of physical parameters.

V_{BI} is determined by the photocurrent alone and remains unaffected by issues that may occur when bias is applied in dark conditions. It is the surest check of a device's performance given that external problems such as parasitic resistances manifest themselves in the dark current and in the V_{OC}.

While V_{OC} often varies from device to device, V_{BI} for the same set of materials and device parameters should be completely consistent unless there has been a physical change made to the device. In our case, we will introduce such a change by placing a physical barrier at the donor-acceptor interface.

V_{OC} can never exceed V_{BI}, so in a way V_{BI} is a measure of the maximum possible voltage the device can generate. The closer V_{OC} gets to V_{BI} the closer the device is to performing at its full potential. It is not always useful to look at V_{OC} alone, given that it varies with device performance in the dark. In conclusion, when we discuss the effect the interstitial concept is having on device performance in Chapter 4, we will observe changes in V_{BI} almost primarily over V_{OC}.

2.4 Bulk vs Planar

The bulk heterojunction (BHJ) device became popular when it became apparent that the free charge generation depended on the interfacial area between the donor and acceptor materials [11]. It is widely accepted that maximizing this interface would allow for a greater area of contact across which charge separation can occur. However, this also means that the free charges generated at these interfaces will encounter more interfaces before they reach the electrodes for the final charge extraction step and therefore may recombine.

We need to find a delicate balance in the morphology because of the competing

rates of recombination and generation. For example, excessive phase segregation can cause geminate recombination while, at the same time, it is important to create percolation channels for charge to travel along [40]. The fact that the exciton diffusion length in most organic materials is in the ball park of 10 nm [8] makes the careful engineering of film morphology even more important. It is complicated to achieve this in a blend device since it is impossible to optimize each material layer on its own. Common approaches to control the morphology in the donor and acceptor material include solvent additives and trying to balance the volume ratios of the two materials. Layer thickness can be optimized independently allowing us to control thickness for different materials according to their diffusion lengths. The rule of thumb is that the thickness of each layer should be on the order of 1/absorption coefficient of the material which would allow it to absorb 63% of the incoming light on the first pass [7]. It is near-impossible to achieve this thickness precision in a bulk device and you have to rely, instead, on material ratios within the bulk.

The planar device, on the other hand can be optimized layer by layer and also allows more freedom in the device architecture itself. The structure lends itself well to the tandem solar cell device concept because it can be used to create multiple junctions. This also means that, as is vital for this work, additional layers can be added to the structure without complications such as solvent incompatibility.

Finally, the planar structure was particularly useful for this work given that there are no changes in morphology that must be accounted for when conducting experiments. We are able to easily vary parameters without worrying about how that will affect the morphology of the materials already present in the active layer.

Chapter 3

Materials and Methods

This work relies heavily on our choice of energetically appropriate materials for our device concept as well as the fabrication techniques needed to build the structures.

Various attempts to create bilayer devices have been made in the past. Azyner et al (2009) successfully created a bilayer device of comparable efficiency to the BHJ. They dissolved the acceptor and donor materials in mutually immiscible solvents and spin coated them consecutively onto the substrate [8]. However, as Lee et al discovered through neutron reflectivity measurements, the PCBM diffuses through the P3HT and becomes more evenly distributed across the film upon annealing, thereby making it similar to a BHJ device [22]. They found that some level of intermixing occurs even without thermal treatment.

Our method of fabrication allows us to utilize solution processed materials that cannot withstand thermal evaporation. For the solution-processed control bilayer, each layer is optimized individually to create films with appropriate phase segregation and thicknesses comparative to the exciton diffusion length. We were then able to easily engineer the interface in our control devices by introducing materials with varying thicknesses and energy states as intermediaries between the donor and acceptor layers.

In this chapter we explain our choice of materials for the donor, acceptor and intermediate materials. We then describe the fabrication processes we created and optimized for the solution processed materials. The vapor deposition process as well

as the characterization briefly mentioned here is described in detail in elsewhere [35].

3.1 Materials

Non-crystalline or amorphous structures contain intrinsic defects which increase the density of traps and recombination centers that gives rise to the following problems [1]:

- Diffusion lengths are shorter. This means the materials' optical absorption properties have to be very strong. This also makes an extended built-in electric field important for carrier collection.
- Intrinsic defects increase parasitic resistances, making carrier density the main factor influencing the electrical characteristics.
- The minority carrier lifetimes and diffusion constant also depend on carrier density.

In keeping with these restraints, the materials chosen for OPV devices must have stronger absorption properties than those of silicon. Higher absorption means that the films can be thinner and so, the short diffusion lengths are not a significant source of loss. A large part of this work was dedicated to optimizing the film thickness and morphology to reduce losses through exciton recombination. For this work, materials were chosen primarily for energy alignment and conductivity.

3.1.1 Solution Processed Control: P3HT and PCBM

The use of polymers in electronic devices took off when Shirakawa, McDiarmid and Heeger discovered that polymers can be highly conductive when halogenated [32]. Their work with polyacetylene brought conjugated polymers into the spotlight for use in flexible, thin electronics that could be cast in solution and roll-to-roll processed.

The family of polythiophenes is one such conjugated polymer that quickly gained popularity for use in optoelectronic devices given its ease of fabrication, good absorption and relatively good solid-state packing [5] We use poly(3-hexylthiophene-2,5-diyl)

(P3HT) as our donor and the popular fullerene derivative, [6,6]phenyl-C61-butyric acid methyl ester (PCBM) as the acceptor in this device structure. PCBM reliably produces high efficiency devices and, unlike fullerenes, it is solution processable.

Later in this chapter we describe how we fabricated a bilayer P3HT/PCBM device using transfer printing. The device serves as our solution-processed control device for the interstitial layer concept.

3.1.2 Dry Deposition Control: Spiro-meOTAD and C60

We chose a pair of materials that are energetically similar to P3HT/PCBM for our second control device. Spiro-meOTAD is a wide-bandgap material with strong conductive properties when annealed in air or doped with lithium salts [44].

These material are vapor deposited, allowing us to create reliable planar structures of very precise thickness. The HOMO level of spiro-meOTAD is comparable to that of P3HT while PCBM is a C60 derivative, making their material properties very similar. The behavior of the vapor-deposited spiro-meOTAD/C60 control device thus makes for a good comparison to use against the P3HT/PCBM solution-processed device.

3.1.3 Interstitial Materials

Lead(II) Sulphide Quantum Dots

Quantum dots (QDs) are versatile semiconducting materials whose electronic properties can be easily engineered to suit our needs. In this work we use Lead (II) Sulphide (PbS) QDs that were synthesized at the Arango Lab. We take advantage of the wide variety of ligand chemistries that are available for QDs and use them to tune the surface properties via ligand exchange [13]. We exchange the long native ligands, oleate (OA) capping ligands (whose insulating properties make them unfavorable for use in photovoltaics) [20], for shorter EDT and TBAI ligands in separate device architecture. These ligands allow for better surface passivation and increased carrier and exciton lifetimes [13]. The shorter ligands allow for better coupling and delocalization between charge carriers. They also improve the mobility and conductivity of the dots.

Wide-bandgap Small Molecule: Alq3

The wide band-gap material tris(8-hydroxyquinoline) aluminium (Alq3) is usually used in electroluminescent devices such as organic light-emitting diodes. Various groups have demonstrated that Alq3 reduces recombination during charge extraction at a LiF/Al interface due to enhanced electron injection [22]. This suggests that it may exhibit similar properties when placed elsewhere in the device architecture. In our case, it was placed at the interface to suppress interfacial recombination and promote charge separation.

3.2 Planar Device Fabrication

A key aspect of the device architecture proposed in this thesis is the planar structure of the acceptor and donor layers. In order to achieve a distinct, planar interface between the materials we needed a fabrication technique that allowed us to deposit solution processable materials in consecutive layers without damaging the preceding layer.

The transfer printing technique described in §3.2.2 of this chapter was optimized for P3HT and PCBM planar cells and was found to be easily replicable for other materials also. The main advantage of this technique is that, with the correct pre-treatment of the stamp, any solution processable material can be transfer printed onto a previously deposited layer in a dry, non-destructive manner.

3.2.1 Optimizing P3HT thickness

In order to minimize exciton recombination, we had to optimize our donor layer - for solution processable materials this process involves finding the exact ratio of solvent, solvent additives, spin-speed and the material itself.

For the bulk device, P3HT and PCBM are dissolved in DCB and spun-cast together. For the planar device, we found that the DCB caused the pristine P3HT layer to crystallize in a way that made the surface too rough for efficient transfer printing

as is apparent by the large domains visible in Fig. 3-1.

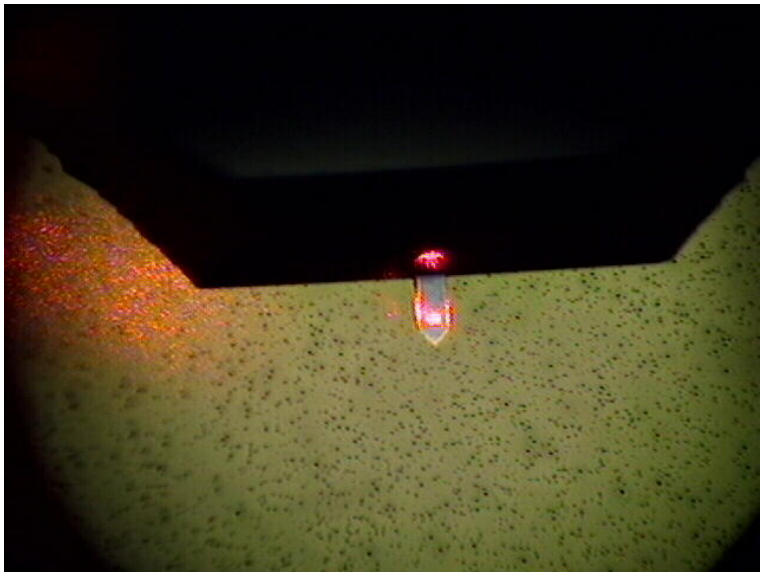

Figure 3-1: An image of P3HT dissolved in 1-2 DCB and spun onto a glass substrate

We processed different weights of P3HT in toluene, 1-2, dichlorobenzene and chloroform as shown in Fig. 3-1 and found the optimal weight to be 5mg per ml of chloroform. The resulting film, when spun at 2000 rpm, had low roughness and a thickness of 20 nm which is appropriate for P3HTs 4-6 nm exciton diffusion length. If we had made the layer any thinner we would sacrifice absorption. Due to chloroform's lower boiling point, in comparison to the other two solvents, the polymer chains have less time to aggregate and form large domains. Aggregates facilitate mobility in the bulk device, but in the planar device they may pierce through the thin layers and cause leakage.

3.2.2 Transfer Printing

We prepared the solution processed planar structure by transferring the PCBM onto the previously deposited P3HT layer. The printing process is detailed in a standard operating procedure in §A.1 and Fig. 3-4. The material to be printed was spun-cast onto a silicon elastomer stamp, polydimethylsiloxane (PDMS). It was then gradually brought into contact with the substrate to minimize trapped air-bubbles. Heat and

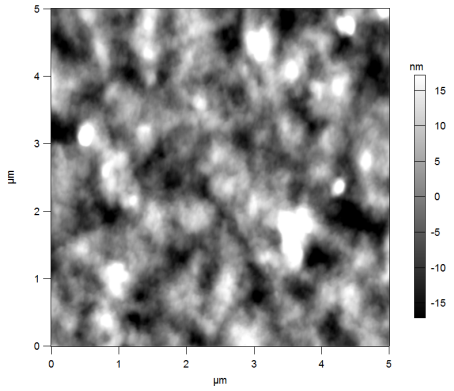

(a) Dichlorobenzene produced large aggregates of up to 15 nm and had an RMS roughness of 8.5 nm

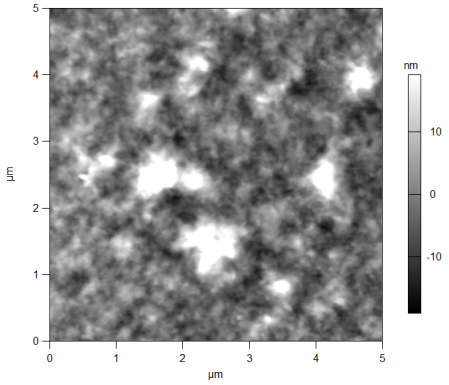

(b) Toluene appeared to create a more disordered film with RMS = 7.5 nm

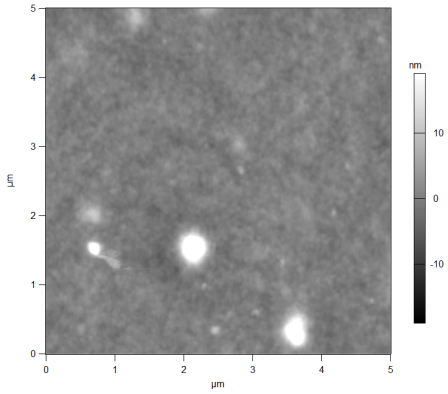

(c) Chloroform produced a film that had much fewer and smaller aggregates and RMS = 1.4 nm

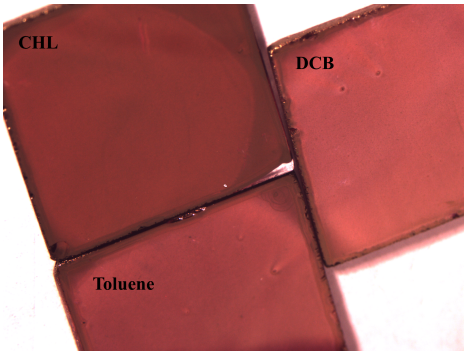

(d) The film processed in chloroform was smoother in general compared to the other two solvents.

Figure 3-2: AFM and camera images of P3HT films spun from different solvents. We used P3HT in chloroform for the pristine P3HT layers in this work.

pressure was then applied to ensure complete transfer and stamp was lifted off the substrate, leaving the spun film printed onto the substrate.

The PCBM solution concentrations commonly used for bulk devices are not compatible with the transfer printing process. In order to maximize surface adhesion between the substrate and the film being printed we had to find a way to minimize material aggregation on the stamp. We found that reducing the concentration by weight of PCBM to 10 mg/ml (compared to the 40 mg/ml used in bulk devices) in chloroform reduced large domains. The stamps were pre-soaked with hexane or octane for 30s that causes the stamp to swell evenly and then pre-wetted with chloro-

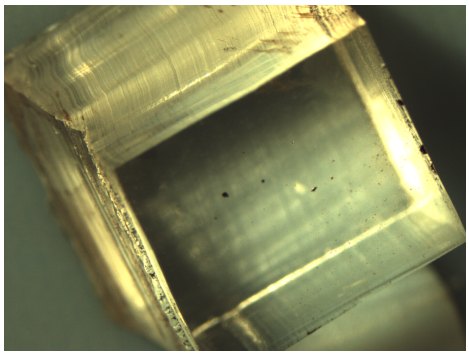

(a) The concentrated PCBM solution formed large domains in the center and did not spread well on the PDMS leading to incomplete printed films and leakage

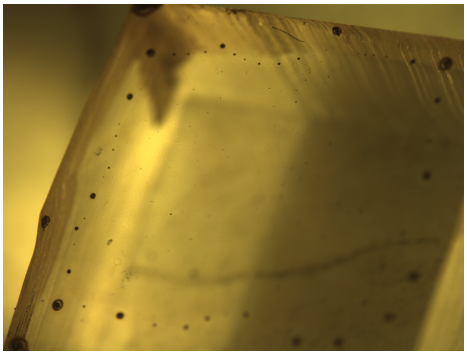

(b) Lowering the concentration of PCBM showed better dispersion on the stamp. The spots on the edges formed due to the swelling of the stamp in the middle but did not affect the active area.

Figure 3-3: PCBM coated on PDMS stamps. (a) is a more concentrated solution coated on a dry PDMS stamp (b) is a more dilute solution coated on pre-soaked and pre-wetted PDMS

form to improve the dispersion of the PCBM film onto the stamp, Fig 3-4 shows the difference between the stamps spun with the original high-concentration solution and the optimized PCBM solution spun on pre-soaked stamps. Finally, we found that the application of heat and even pressure led to a complete transfer of the film.

Since thicker films lead to incomplete printing, we stamped two thin films of PCBM consecutively to achieve comparative thickness.

3.3 Deposition of QDs

The Lead(II)Sulphide QDs with OA ligands are suspended in octane. They are transfer printed at the interface of the devices and the native ligands are exchanged with for EDT or TBAI ligands before they are printed. The TBAI ligands were suspended in methanol. The EDT ligands, however, were suspended in acetonitrile. The acetonitrile appears to completely remove or damage the spiro-meOTAD donor film during ligand swap.

To prevent damage to the spiro-meOTAD layer, we treat the PbS film on the

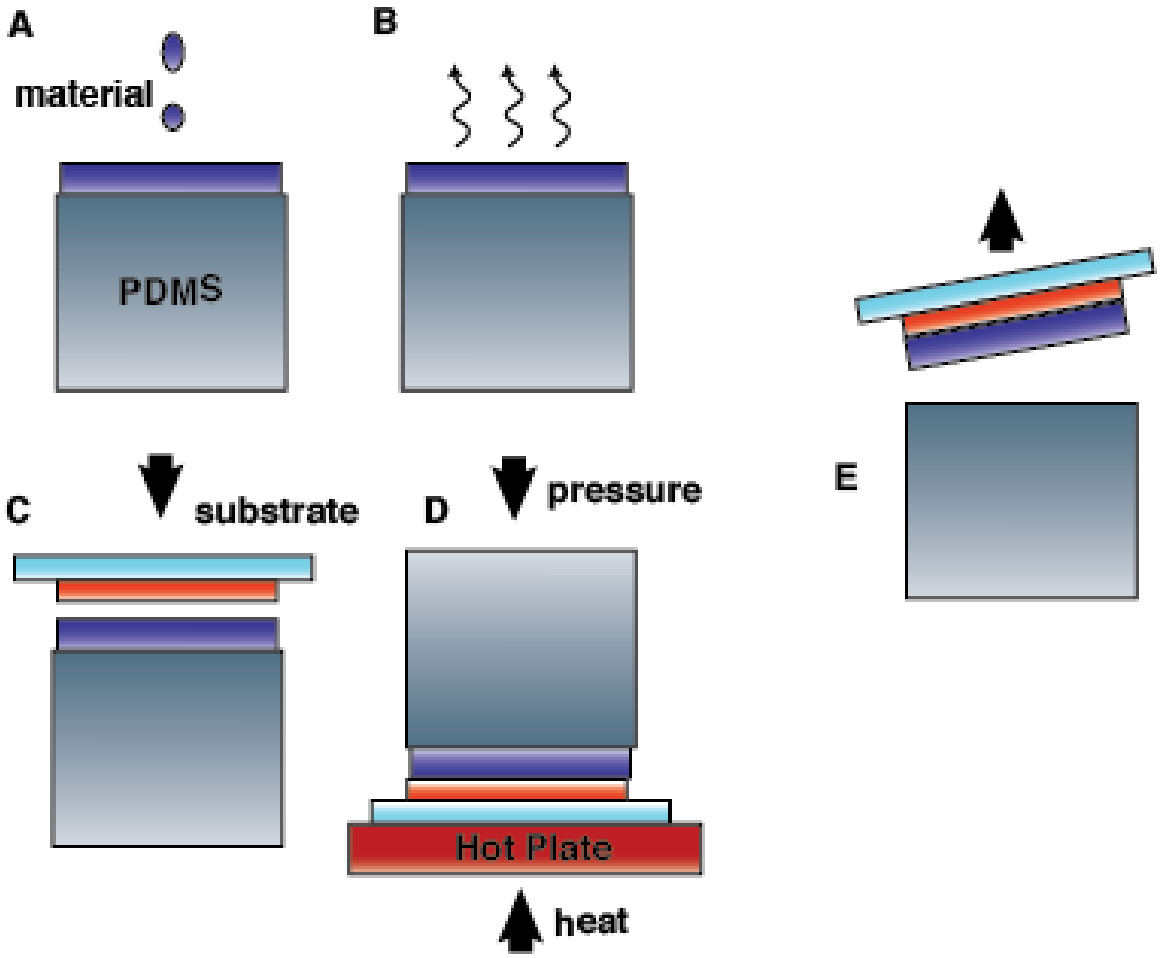

Figure 3-4: The transfer printing process: (A) First the PDMS stamp is presoaked with a solvent that allows it to swell uniformly, next it is pre-wetted with the solvent that the material being deposited is dissolved in. Finally the material itself is spin-cast onto the stamp. (B) The stamp is allowed to dry under vaccuum for 30 minutes to remove any remaining solvent. (C) The substrate, with previously coated material on it is brought into contact with the material spun onto the surface of the stamp. (D) Pressure and heat is applied for 30 -60 s. (E) The printed material transfers completely onto the substrate and the stamp can be popped off in a single, fluid motion.

PDMS stamp prior to printing. The QD films are then annealed in air for 30 minutes at 110C. Devices with a P3HT donor are not air-annealed since P3HT photooxidizes.

An additional technique used to deposit the QDs was spray-coating. This fabrication technique involves using an airbrush to deposit the QD in the form of a fine mist that settles onto the substrate. [21]. We suspect that this method of deposition may be damaging previously spin-cast layers given that the octane makes contact with the donor material. The ligand swap that follows is removing part of the previously deposited layer and may be the cause of low V_{OC} in some of our devices.

In the future, pairing the printing process with the spray deposition could allow us to protect the donor film. The printed QD film creates a layer that coats the donor material and protects it from the solvent in the spray and the ligand swap. We have not, however, been able to obtain reliable results using this method.

Chapter 4

Results and Discussion

4.1 Results

We present a device that demonstrates extremely high J_{SC} but low V_{OC}. We believe the spray deposition fabrication technique used to deposit the QD layers in the device may be damaging the hole transport layer, hence lowering V_{OC}.

Next, we describe an interstitial device concept that raises V_{BI} above the theoretical limit, but sacrifices J_{SC} to do so. The challenge that presents itself is finding a way to combine the beneficial aspects of the two device concepts to produce a high efficiency device.

Finally, we investigate four donor-acceptor pairings with PbS QDs printed at the interface. For the most part, we compare how the V_{OC} and V_{BI} vary as we utilize QDs with different ligands as interstitial materials.

4.1.1 High J_{SC} device with thick QD layers

Fig. 4-1a describes a device that produced a relatively high J_{SC} of 12 mA/cm^2. The device was comprised of four layers of PbS QDs that were spray coated between a pair of transport layers, Spiro-meOTAD and C60. The native OA ligands were swapped out for EDT ligands for the first two layers and TBAI ligands for the last two layers. However, the device produced a low V_{OC} of only 0.29 V. The low V_{OC} can, in part, be

(a)

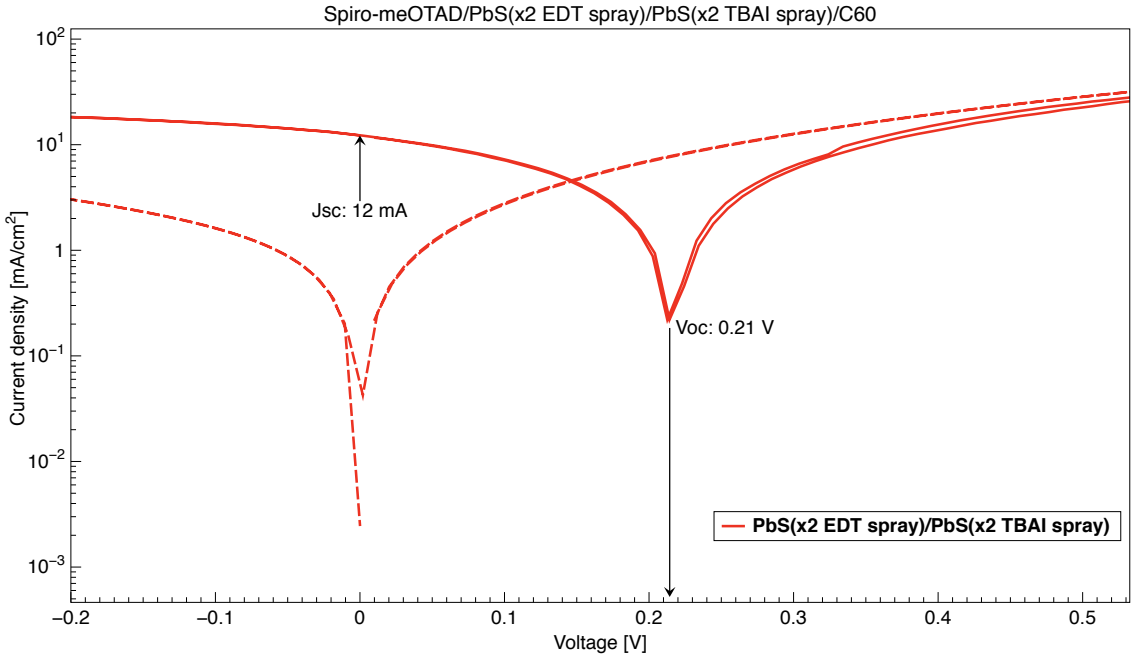

(b)

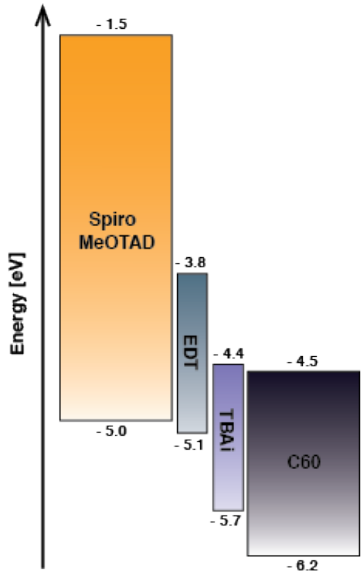

Figure 4-1: (a) The log-linear IV characteristics of the high-J_{SC} PbS QD device are pictured here. The black curve is device performance in the dark while the red is its performance under illumination. The device generated a J_{SC} of $12mA/cm^2$, but a V_{OC} of only 0.29 V. A damaged or incomplete hole-transport layer may have lead to this low V_{OC}. (b) The device's architecture is shown here. Two spray deposited layers of PbS-EDT QDs followed by two layers of PbS-TBAI QDs were sandwiched between Spiro-meOTAD and C60 transport layers.

attributed to the QD spray deposition process that may have damaged the thermally evaporated hole transport layer. The high dark current (black curve) points to this conclusion.

4.1.2 High V_{BI} device with wide-bandgap interstitial layer – proof of concept

For device architectures that rely on interfacial kinetics, one would expect that modifying the interface with a thin interstitial layer would affect the device performance. We constructed a device consisting of P3HT and C60 and introduced a barrier at the interface that would potentially suppress CT state recombination and raise the V_{OC}. We chose Alq3, a wide-bandgap small molecule with good conductivity and vapor deposited it at the P3HT/C60 interface.

The IV characteristics of this device are shown in Fig. 4-2a. The interfacial bandgap of the P3HT/C60 donor-acceptor pair suggests a maximum V_{OC} of 0.4 V but our devices produced only 0.2 V. Inserting 1 nm of Alq3 at the interface raised the V_{OC} to 0.27 nm, while 2 nm raised it to 0.4 V - which is right at the theoretical limit for this donor-acceptor pair. However, the V_{BI} suggests that this device architecture can potentially produce a voltage of 0.52 V, which would put its performance above the theoretical limit.

Unfortunately, the J_{SC} fell consistently with rising V_{OC} and the 1.2 mA produced by the P3HT/C60 control device dropped to 0.05 mA for the 2nm Alq3 device. There also appears to be a strong thickness dependence for the Alq3, as the V_{BI} began to drop for 3 nm.

The results suggest that, by altering the interface, we can not only suppress interfacial recombination, we can push the V_{BI} above the HOMO-LUMO limitation, although the V_{OC} remains at the HOMO-LUMO limit. The low J_{SC} can be attributed to poor electron transfer from P3HT to Alq3 to C60.

(a)

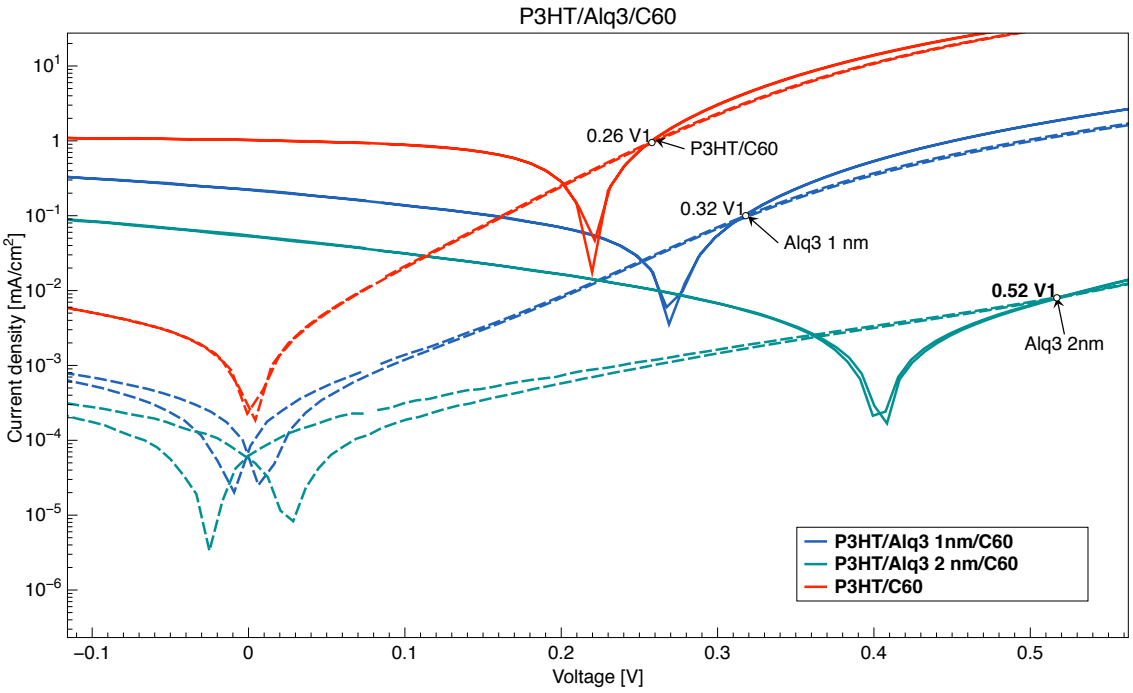

(b)

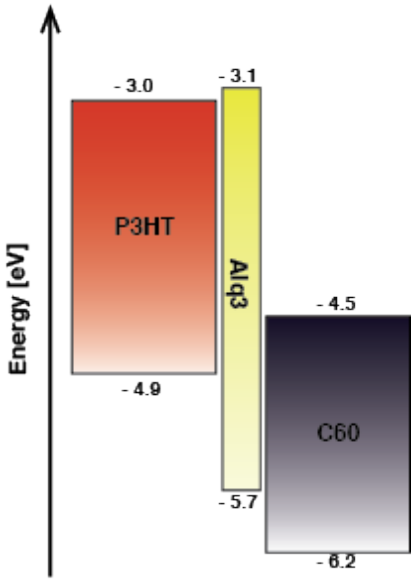

Figure 4-2: (a)Varying thicknesses of Alq3 were placed at the interface of a P3HT/C60 planar device. The teal curve in this figure is a device with 2nm of Alq3 at the interface that demonstrates a V_{BI} of 0.52 V - this is above the 0.4 V theoretical limit for the P3HT/C60 donor-acceptor pair. (b) The device concept for this device employs a wide-bandgap material (Alq3) that suppresses recombination at the interface.

4.1.3 PbS QD interstitial layer in a solution-processed bi-layer device

To address the issue of poor electron injection across the interfacial layer, we chose a material with a more favorable energy alignment. We employed the interstitial layer concept and used transfer printing to deposit thin films of PbS QD on top of the P3HT layer and completed the active region with two printed layers of PCBM as the acceptor.

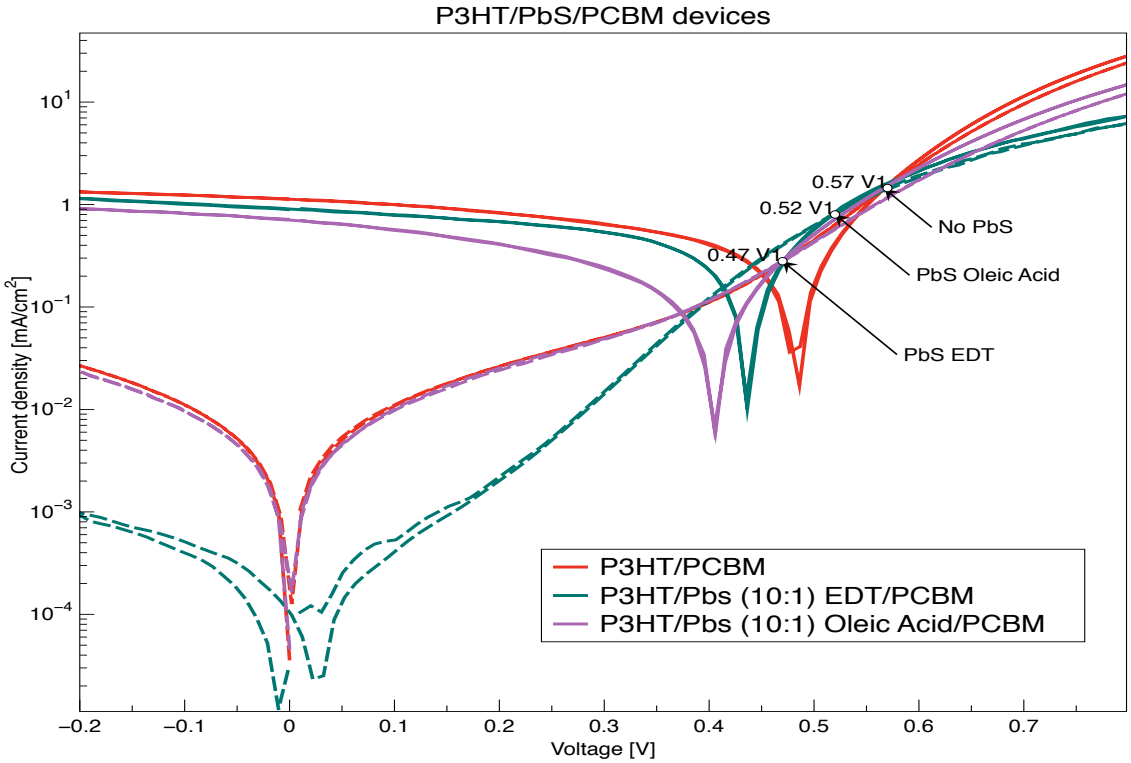

(a) PbS with native OA ligands and PbS with EDT ligands were placed at te interface of a P3HT/PCBM planar device. In both cases, the QDs affected the V_{BI} negatively. The PbS EDT device, however, improved dark current dramatically.

An advantage of using the QDs is that we can shift their energy levels by simply swapping out the ligands attached to the surface of the dot. Fig. 4-3a summarizes the effect of thin layers of PbS with native OA ligands (purple curve) and with EDT ligands (teal curve) printed at the interface. Contrary to expectation, the QDs lower V_{OC} and J_{SC} universally. The reduction in V_{OC} is puzzling. It is possible that the QDs are enhancing recombination instead of suppressing it.

(a)

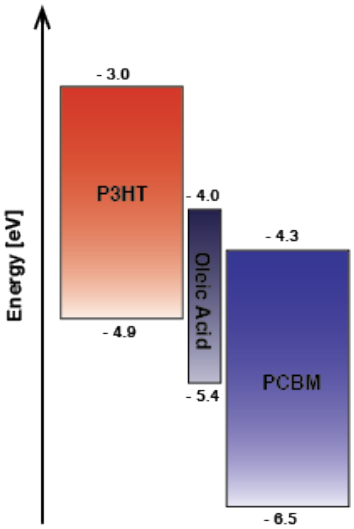

(b)

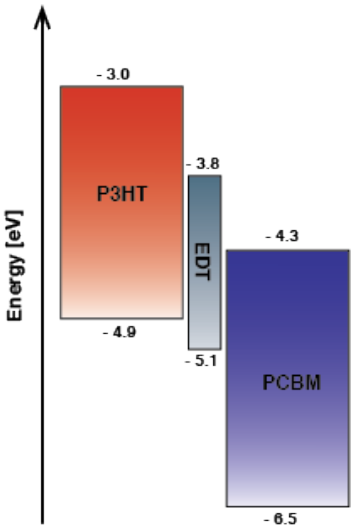

Figure 4-4: (a) Device structure for PbS OA interstitial layer devices. These ligands tend to be too insulating to be used in photovoltaics. (b) Device structure for PbS EDT interstitial layer devices. The EDT ligand swap and acetonitrile rinse was performed on the film since acetonitrile did not appear to damage the P3HT layer.

4.1.4 PbS QD interstitial layer with printed, solution-processed acceptor layer

To investigate the interaction between the hole transport layer and the QDs, we replace P3HT with a more conductive, wide-bandgap hole-transport material - spiro-meOTAD - the same material used in the high-J_{SC} device. We then carried out the same experiment described in the previous section.

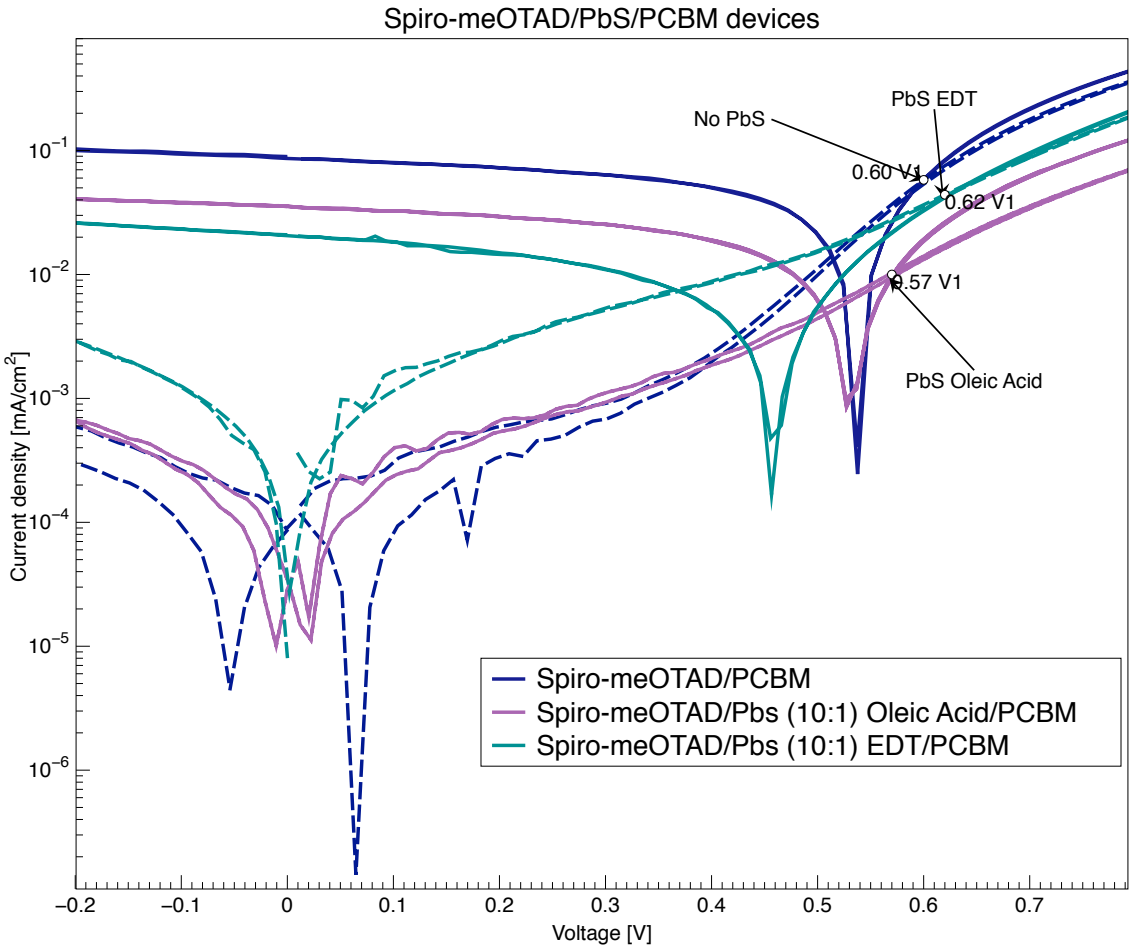

(a) Devices are identical to those presented in Figure 4-3a but with Spiro-meOTAD as the donor material this time. This time, the PbS EDT lowered J_{SC}, V_{OC} and dark current, but raised V_{BI} by a small amount. The PbS OA lowered V_{OC} and had a similar effect in this device architecture as it did on the the P3HT/PCBM cell.

This time, the PbS EDT lowered J_{SC}, V_{OC} and dark current, but raised V_{BI} by a small amount. The PbS OA lowered V_{OC} that is probably due to the insulating ligands and leakage in forward bias. There is the possibility that printing the acceptor

material onto the QD layers was damaging them. It is also possible that the energy alignment of the spiro-meOTAD/PbS interface is not sufficiently spaced to allow efficient charge transfer (Fig. 4-6b).

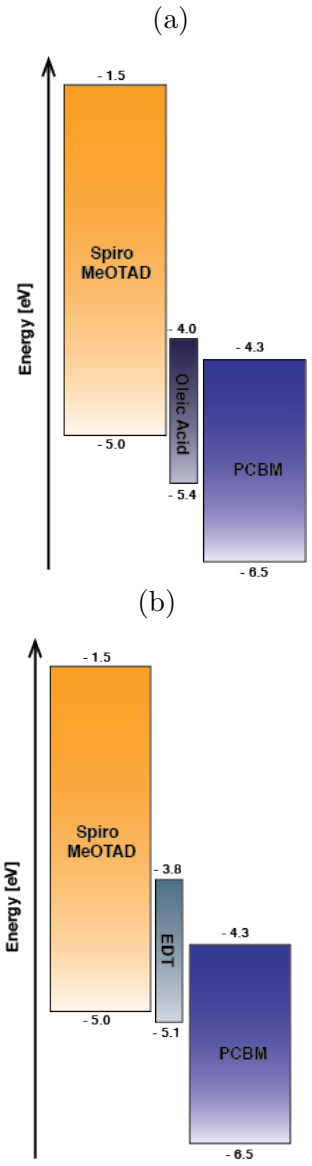

Figure 4-6: (a) Device structure for the PbS OA devices. (b) Device architecture for the PbS EDT interstitial layer device. Notice that the HOMO levels for spiro-meOTD and EDT are almost level, which may account for the low J_{SC}.

4.1.5 PbS QDs interstitial layers in dry-deposition bilayer device

We now turn to the donor-acceptor pairing employed in the high-J_{SC} QD device described in Section 4.1.1. The experiments described in this section were an attempt to narrow down the source of V_{OC} loss in that device. The the high-J_{SC} QD device was comprised of thick layers of PbS EDT QDs and PbS TBAI QDs between spiro-meOTAD and C60 transport layers. Unlike the previous devices, the devices in this section were annealed in air at 110C after QD deposition. We believe air annealing causes the PbS to oxidize and shrink a little, enlarging the band-gap, which would help with energy level alignment.

We experimented with thin, printed layers of PbS QDs with both TBAI and EDT at the interface and observed conflicting results. Fig. 4-7a shows the IV characteristics of the devices with PbS TBAI. While there was a promising result of improved V_{BI} and J_{SC} from the thin layer of PbS TBAI (teal), the device still demonstrated a poor fill factor due to bad shunt resistance.

It is also important to mention that the spiro-meOTAD/C60 control device usually has a higher V_{BI} and J_{SC} of 0.66 V and 1.25 mA/cm^2 as compared to the 0.6 V and 0.8 mA/cm^2 demonstrated by the control device in this experiment. When this inconsistent behavior of the control device is taken into account, it appears that the thin layer of PbS TBAI is only adding to the shunt resistance and is leaving V_{BI} and J_{SC} unchanged.

We also see a dramatic decrease in J_{SC} for the thick PbS TBAI device (purple). This may be a consequence of annealing, treating and transfer printing the thick film which appeared to collectively produce cracks in the film.

(a)

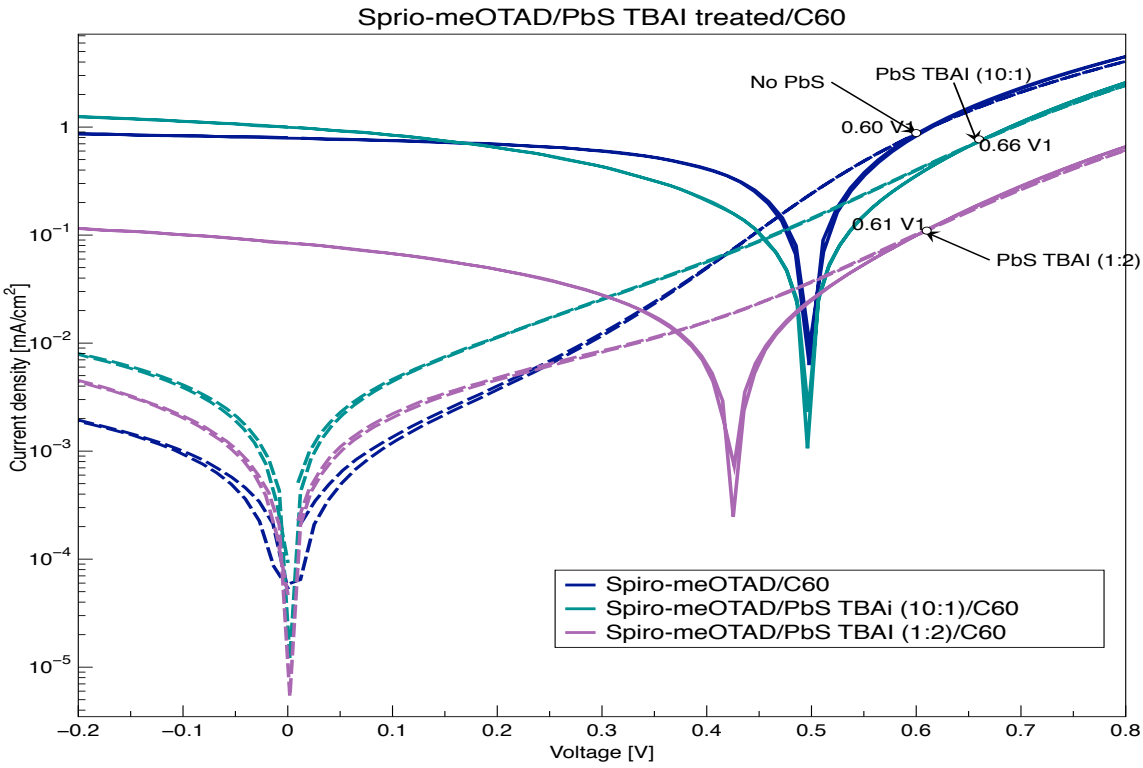

(b)

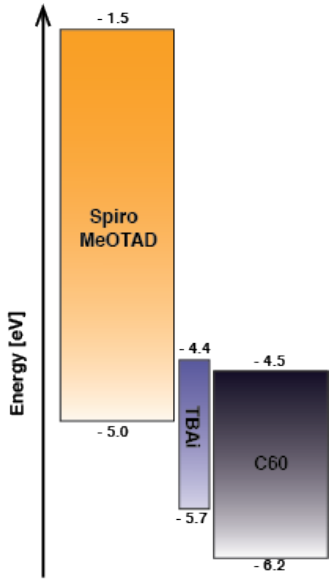

Figure 4-7: (a) PbS TBAI ligands of various thicknesses were added to the interface of a Spiro-meOTAD/C60 device. The thin layer of TBAI had little effect on V_{OC} but raised V_{BI} and J_{SC}. The thick layer, however brought all three back down. This drop in J_{SC} may be due to crack formation in the thick PbS TBAI layer. (b) The device structure for the PbS TBAI interstitial layers. These devices were annealed in air for 30 mins after the QDs were printed which improves J_{SC}.

(a)

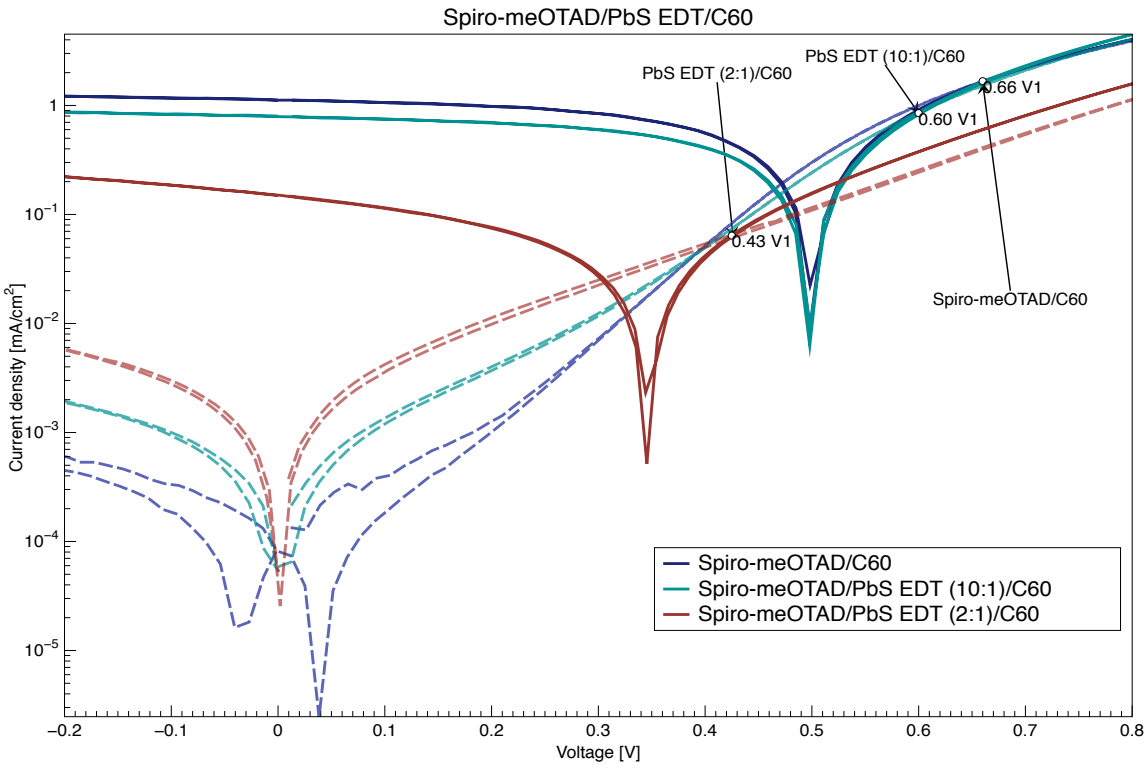

(b)

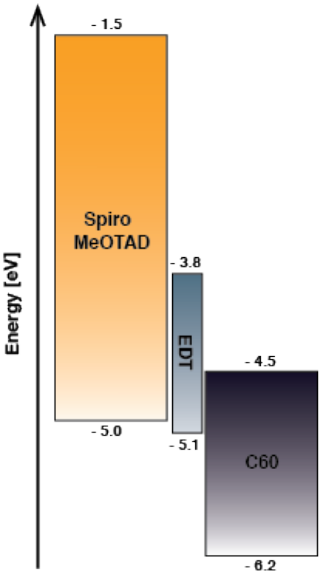

Figure 4-8: (a) These devices exhibit varying thicknesses of PbS EDT at the interface of a Spiro-meOTAD/C60 device. The devices exhibit lower V_{OC} and J_{SC} with increasing thickness. We also see lower dark current and greater leakage in forward bias for the thickest device (maroon). (b) Device architecture: Layers of PbS EDT were transfer printed at the interface of a device with a high-conductivity donor (Spiro-meOTAD) and a fullerene acceptor.These devices were annealed in air for 30 mins after the QDs and PCBM were printed.

4.2 Discussion

To evaluate the data presented in the previous section, we compare comparing the V_{BI} demonstrated by each device against the theoretical limit for V_{OC} as suggested by the HOMO-LUMO difference between donor-acceptor pairings. The results are summarized in Fig. 4-10.

It is interesting to note that TBAI ligands on a thin PbS layer potentially improve V_{BI} but taking into account the anomalous behavior of the control device for that experiment negates the credibility of this result. Additionally, the fact that thickening the layer lowers V_{BI} and J_{SC} supports the conclusion that, as a whole, PbS TBAI layers are affecting V_{BI} negatively. Thin layers of EDT QDs again seemed to have little to no affect on the V_{BI} but thicker layers lowered the V_{BI} once more.

It is important to note that the spiro-meOTAD/C60 control device falls well above the theoretical limit, potentially pointing to an error in the HOMO-LUMO values in the literature or a fabrication error. Regardless, we see a trend of decreasing device performance with increasing thickness for both the ligands. This is inconsistent with the theory that states that the limit on V_{BI} and hence V_{OC} is set by the HOMO-LUMO offset between the donor and acceptor, which in this case, remains unchanged.

The P3HT/PCBM donor-acceptor pairing has a theoretical limit of 0.6 V, while pairing spiro-meOTAD with PCBM should give a maximum V_{BI} of 0.7 V. In the experiment to investigate donor-PbS interaction, we compared thin layers of the longer native OA ligands to shorter, more ligands that made the dots more conductive. The results we obtained for the two donors were contrasting. For the P3HT/PCBM solution-processed device, both types of ligands lowered V_{BI}. The EDT ligands performed worse than the OA ligands. However, when placed on spiro-meOTAD, the EDT ligands raised V_{BI} a little while the OA ligands had a negative effect on it. This can attributed to how the two different ligands behave with the two different donor materials.

Different QD ligands altered the V_{BI} noticeably as did varying the thickness a of the same ligand. The data does not point to a clear trend as to how V_{BI} correlates

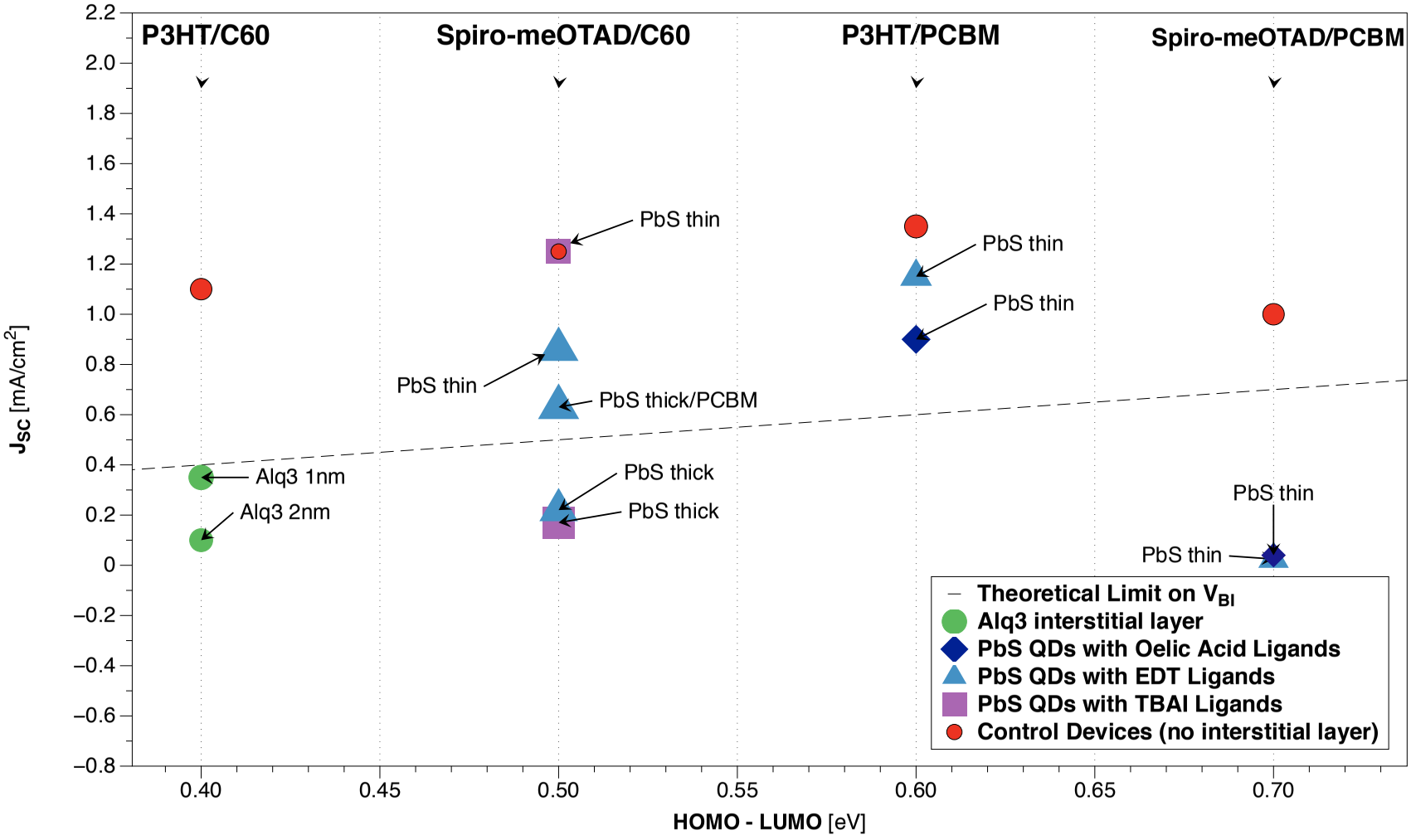

Figure 4-9: J_{SC} vs the HOMO-LUMO difference for all the donor acceptor pairings and interstitial concepts tested in this work. The prime take away is that, with the exception of the thin PbS TBAI device, J_{SC} always suffers in the presence of an interstitial material.

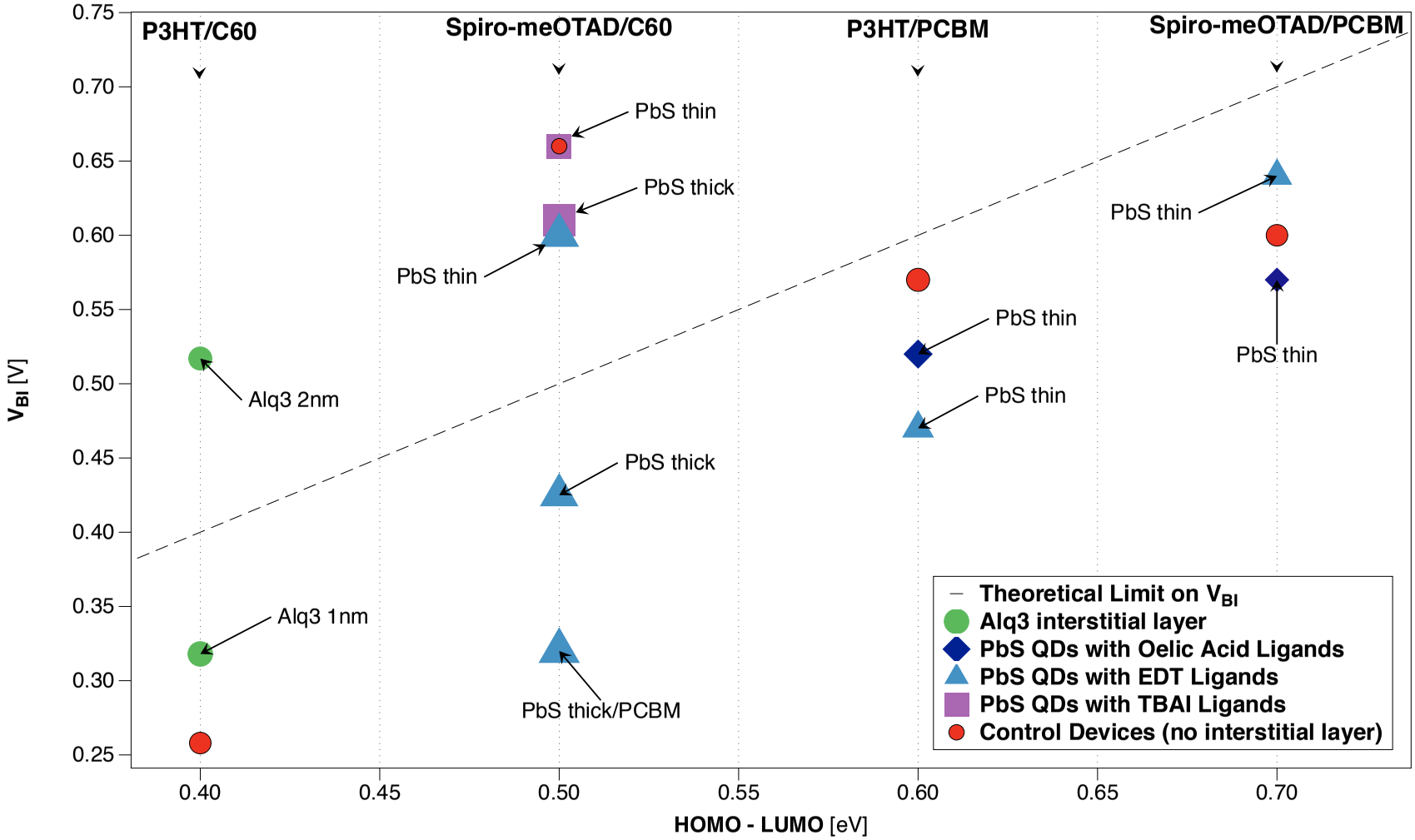

Figure 4-10: V_{BI} vs the HOMO-LUMO offset of all the donor-acceptor pairings tried. The Aq3 2nm devices was the only one that raised V_{BI} over the theoretical limit. The thin PbS EDT layer in the Spiro-meOTAD/PCBM device showed an insignificant increase in V_{BI} and a lowered V_{OC}. The thin PbS TBAI device was the only one that improved V_{BI} and J_{SC} but left V_{OC} unchanged.

with the ligands used. For example, more conductive, EDT ligands behave differently with P3HT than with spiro-meOTAD. A definite conclusion, however, is that engineering the interface with different interstitial materials changes V_{BI} in a way that is inconsistent with the existing theory.

It is hard to extrapolate a distinct trend from these data points given the inconsistency in device behavior. Physical issues such as shorts and parasitic resistances in the device should not affect V_{BI} as V_{BI} depends on photocurrent. Photocurrent describes the fundamental behavior of the device's behavior under illumination regardless of how it behaves under bias in the dark. On principle, it should not change unless there is a physical change in the device that is affecting the photocurrent. We can make the claim that the introduction of QDs at the interface is one such physical change that alters V_{BI}. The inconsistency in these changes to V_{BI}, however, is harder to justify.

4.2.1 Effects of fabrication variations on device performance

There appears to be a strong correlation between fabrication techniques and the change in V_{BI}. The processes of swapping ligands and applying heat and pressure during printing are hard to reproduce exactly every time. These fabrication processes vary from device to device and are likely changing the way each device behaves. The two most probable scenarios are that our methods are either affecting recombination at the interface or are shifting the energy levels of the materials.

The transfer printing process has been optimized for PCBM printing and not for treated QDs. For example, we observed lower adhesion between ticker layers of EDT treated QDs and the spiro-meOTAD and we were unable to print them entirely. While thick PbS TBAI layers printed well, the films appear to be shrinking when the OA ligands are replaced with shorter TBAI ligands. This seems to be and causing cracks in the film that become even more pronounced after air-annealing. As a result, thick layers of TBAI show signs of extensive cracking which could be a source of leakage leading to low V_{OC} and J_{SC}.

One possible explanation for the varying V_{BI} is that the print deposition method

shifts energy levels in a way that is not even on both sides of the interstitial layers. This could be bringing about a change in the interfacial band-gap and hence the V_{BI}. The data, however, shows that we cannot think about it in the simple HOMO-LUMO offset model.

Another scenario — in keeping with the recombination rate model for V_{BI} — is that the different ligands are changing the recombination rate at the interface that is another fundamental process in the device that would change the V_{BI}. It possible that the ligand treatment is not seeping through the entire QD layer leaving the film altered in certain areas and not in others. Hence, when we print the film, it is possible that the acceptor material is making contact with a different ligand as compared to the donor material. This would result in a change in conductivity and a change in how recombination would occur in these films. If the transfer printing technique is not replicated exactly every time this could be a source of inconsistency in behavior from device to device and even from pad-to-pad within the same device.

Finally it is possible, for the thicker devices that we are seeing recombination within the bulk of the QD layer. This could be a result of defective QDs and poorly bound ligands. For a thicker film defect states would bring down V_{BI} whereas we would see fewer defects in a thinner film and that would result in higher V_{BI}. This would explain why the thick, high J_{SC} device demonstrated lower V_{BI}.

Chapter 5

Conclusion and Future Work

In conclusion, we present a transfer-printing technique that allows us to fabricate a planar structure for any solution-processable material. We have also demonstrated proof of two separate device concepts: a high J_{SC} QD device and a high V_{BI} thin-film interstitial layer device.

Our high-J_{SC} QD device demonstrates low V_{OC} and high dark current which we attribute to incomplete hole-transport layers. The high V_{BI} thin-film device, conversely, generates low J_{SC}, probably a result of placing a wide-bandgap material at the interface and hindering charge separation.

Our attempts to narrow down the source of low V_{OC} in the high J_{SC} QD device has revealed some interesting device behavior that redefines the way we think about the limitations on V_{BI} and V_{OC}.

We can safely say that there is a way to suppress recombination rates at the interface and to bring the V_{OC} to the point where it surpasses the dependence on interfacial bandgap.

5.0.2 Future Work

This document summarizes the initial results of a work in progress. The next step is to try to refine fabrication techniques to address the issues mentioned in the previous chapter.

In order to achieve high efficiency, we need be able to retain the high J_{SC} generated by the spray-coated QD device while boosting the V_{OC} by finding a way to protect the hole-transport layer.

Our work here proves that we can produce reliable, printed layers of QDs in completely dry conditions. The ligand swap can also be conducted on the PDMS stamp prior to printing. The goal now is to find a way to print a pre-treated PbS QD layer that can coat and protect the hole-transport layer prior to spray coating.

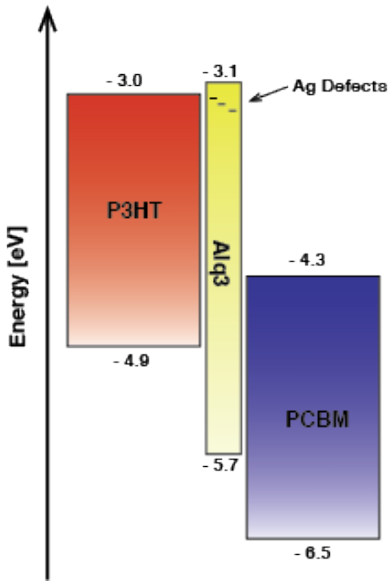

Figure 5-1: Adding a small amount of metal to the Alq3 layer might improve charge extraction and hence J_{SC}

Troubleshooting the high-V_{BI} Alq3 device is another route to pursue. The device demonstrates low J_{SC}, probably due to poor electron injection through the Alq3 layer. One way to promote charge injection is to introduce defect states in the Alq3, possibly through slight doping with silver or aluminum (see Fig. 5-1). Alq3 is a common material used in OLEDs and it is believed that it facilitates charge coupling between the organic interface and the electrode thus improving charge extracting. Lee et al demonstrated that a thin layer of Alq3 at the electrode-organic interface improves OLED performance. It may be possible to deposit a thicker, metal-doped layer of Alq3 at the interface and observe a similar improvement in charge extraction.

If we are able to pair the deposition methods and optimize the interstitial layer

thicknesses, it is possible to have the V_{OC} match the high J_{SC}. This could boost QD photovoltaics to an unprecedented efficiency and change the way we think about these devices altogether.

Appendix A

Standard Operating Procedures

A.1 Transfer Printing

This document describes the standard procedure for depositing a solution-processed thin-film onto a substrate via transfer printing. This fabrication method makes it possible to dry-deposit a solution-processed material without damaging a previously deposited film.

The procedure outlined here has been optimized for stamping P3HT, PCBM and PbS quantum dots onto an ITO glass substrate already coated with a film. Other procedures referenced in this document including the method for preparing PDMS stamps, solutions, spin coating and ligand swap are are described elsewhere.

A.1.1 Hazards

- When working with chemicals in the wet glovebox, put on the appropriate safety gear including goggles, lab coats, and gloves.
- Wear latex gloves on top of glovebox gloves for extra protection
- Before the use of any chemicals in the glovebox, circulation must be turned off (F5).
- Before working with substrates:

  - Turn on HEPA filter to ensure that the atmosphere in the glovebox is free of particles
  - Clean the glovebox by blowing pressurized nitrogen towards the back of the glovebox.
  - Clean the gloves by picking up dust particles with the lint roller.

- Do not touch hot plate while applying pressure during transferring process.
- Keep all needles capped at all times that they are not in use.

A.1.2 Supplies

- Clean substrates in fluoroware
- Micropipette and tips
- Plastic-coated tweezers
- Aluminum foil
- Texwipe (to clean spin coater)
- Timer (annealing)
- Needles and 1 ml syringes
- Clean PDMS stamps
- 2 μ organic filter

Chemicals

- Chlorofom
- Octane
- PbS in Octane

- PCBM 10 mg in Chloroform
- EDT in Acetonitrile
- Acetonitrile rinse

A.1.3 Procedure

- Glovebox Preparation
  - On a sheet of aluminum foil lay out all supplies to be brought into the glovebox. This may include labelled syringes and needles for extracting solvents from jars stored in the glovebox.
  - If the solution to be spin-coated is in an opaque jar, you may transfer the approximate amount needed into a colorless vial to see clearly. Label the vial and place in vial tray.
- Set the spin coater
  - To change a parameter starting at Recipe 1: Press MODE, use the left or right arrow to navigate between the listed parameters (step, ramp, rpm, etc.) and use the up or down arrow to set a desired value, press ENTER, press MODE
  - Parameter settings:
    - Step: 1
    - Ramp: 0
    - RPM (revolutions per minute): For PCBM and PbS set to 1000 rpm
    - Dwell (how long the substrate will spin): 60 s
    - Disp (dispense): none
    - Time: 0 (60 seconds is standard)
- Preparing stamp

- Using wide-mouthed plastic tweezers, carefully lift the PDMS stamp from the base of the stamp so as to avoid damaging the surface. Place stamp onto the o-ring of the spin-coater, center. [1]
- Open the glass cover to the spin coater
- Pre-soak: Load a syringe with octane and, holding the syringe about 5 mm from the surface of the stamp, thoroughly cover the surface of the stamp with octane. [2] Allow the stamp to soak for 30 s and spin to remove the solve.
- Pre-wet: For a other solution processed material, pre-wet with the solvent it is dissolved in. For PCBM or P3HT, repeat last step with chloroform. Allow to sit for 10- 15 s. Spin off for just 15 seconds so surface is still wet for spin coating.
- Depositing solution: In the same method of deposition described above, deposit the solution to be transfer printed onto the surface of the stamp. For PCBM, deposit through the 2 μ filter because it tends to form aggregates. For PbS, you can use the micropipette but make sure the solution covers the surface well. Allow solution to sit for 5 seconds and spin.
- For PbS, you might need to swap out the native ligands for either TBAi or EDT. To do this, deposit the previously prepared EDT and Acetonitrile solution onto the top of the stamp, allow to sit for 30 s and spin. Follow this with the Acetonitrile rinse, allow this to sit for 5 seconds and spin.
- Place stamp back into the labelled petri dish. Place in anti-chamber for 30 minutes and

• Transferring Stamp

- Set the hot plate to 110 C and allow it to heat up.

[1] If the stamp is not centered on the chuck properly, or if the chuck is saturated with solvent from the pre-soak, the vacuum will not form and the stamp will fly off the chuck during spinning

[2] The surface tension of the stamp will cause the octane to draw up to the center, away from the edges, depositing from close to the surface will distribute the octane over the entire surface and ensure even swelling.

- Place the substrate onto the hot plate for 30s.
- Using wide tweezers, place the spin-coated stamp onto the lid of the petri dish. Do not make contact with the surface or the top of the stamp, handle the base only. Gently squeeze and press down with the tweezer to make sure the stamp sticks to the lid.
- Lift substrate off the hot plate and center the ITO over the stamp, place it face down onto the stamp. Using tweezers, push down onto the substrate starting with one corner and working your way over the entire ITO, pushing out any air-pockets that might form between the substrate and the stamp.
- Using wide tweezers place the substrate (now stuck to the stamp) onto the hot plate. Push down on the bottom of the stamp using the tweezers and apply even pressure onto the substrate. Hold for 30 s.
- Remove from hot plate and replace the stamp back onto the petri dish lid. Push down on substrate again, making sure the ITO area is free of air bubbles.
- Grab a corner of the substrate and try to pop the substrate off the stamp. You may need to hold the stamp with the wide tweezers for this.

- Cleaning up
  - Make sure all vials and containers are closed and wrap parafilm on all the vials you used/opened. Wrap the film in the same direction that the cap closes, stretching it as you go around.
  - Change the foil in the spin coater and clean the metal disk with a wipe, removing any material on it.
  - Turn off the HEPA filter once substrates are no longer exposed
  - Auto-purge (F6) (set for 10 minutes) once or twice depending on how long you've been working with solvents
  - Remove all waste to the fume hood and dispose of contaminate items in the hazardous waste container

- After auto-purge has completed, turn on circulation (F5) and ensure that oxygen and moisture ppm's are at zero

Bibliography

[1] Jenny Nelson, *The Physics of Solar Cells*, Imperial College, UK.

[2] *Human Development Report 2009 - Population living below* $2 *a day*, undp.org (2009).

[3] *"WMO Climate Normals for KARACHI (AIRPORT) 19611990"*, National Oceanic and Atmospheric Administration (2014).

[4] *Karachi Electric - Business Generation*, www.ke.com.pk (2015).

[5] Advances in Polymer Science 265, *P3HT Revisited from Molecular Scale to Solar Cell Devices* (Sabine Ludwigs, ed.), Springer.

[6] Firoz Ahmad, *Solar Radiation Studies at Karachi Pakistan*, University of Karachi, Department of Physics, xviii.

[7] Alexi C Arango, *High open-circuit voltage in heterojunction photovoltaics consisting of a printed colloidal quantum-dot photosensitive layer*, MIT Thesis (2010).

[8] Alexander L Ayzner, Christopher J Tassone, Sarah H Tolbert, and Benjamin J Schwartz, *Reappraising the Need for Bulk Heterojunctions in Polymer Fullerene* $Photovoltaics_{T}heRoleofCarrierTransportinAll - Solution - ProcessedP3HT - PCBMBilayer....pdf$ (2009), 20050–20060.

[9] Paul W M Blom, Valentin D. Mihailetchi, L. Jan Anton Koster, and Denis E. Markov, *Device physics of polymer:Fullerene bulk heterojunction solar cells*, Advanced Materials **19** (2007), no. 12, 1551–1566.

[10] Deniz Bozyigit, Sebastian Volk, Olesya Yarema, and Vanessa Wood, *Quantification of deep traps in nanocrystal solids, their electronic properties, and their influence on device behavior*, Nano Letters **13** (2013), no. 11, 5284–5288.

[11] Jean-Luc Brédas, Joseph E Norton, Jérôme Cornil, and Veaceslav Coropceanu, *Molecular understanding of organic solar cells: the challenges.*, Accounts of chemical research **42** (2009), no. 11, 1691–1699.

[12] Alejandro L Briseno and Peidong Yang, *Optoelectronics: Combining chemical worlds.*, 2009.

[13] Patrick R. Brown, Donghun Kim, Richard R. Lunt, Ni Zhao, Moungi G. Bawendi, Jeffrey C. Grossman, and Vladimir Bulović, *Energy level modification in lead sulfide quantum dot thin films through ligand exchange*, ACS Nano (2014).

[14] Lichun Chen, Patrick Degenaar, and Donal D C Bradley, *Polymer transfer printing: Application to layer coating, pattern definition, and diode dark current blocking*, Advanced Materials (2008).

[15] Brian A. Gregg, *The Photoconversion Mechanism of Excitonic Solar Cells*, MRS Bulletin, 2005.

[16] Alexander W. Hains, Ziqi Liang, Michael a. Woodhouse, and Brian a. Gregg, *Molecular semiconductors in organic photovoltaic cells*, Chemical Reviews **110** (2010), no. 11, 6689–6735.

[17] Masahiro Hiramoto, Hiroyuki Fukusumi, and Masaaki Yokoyama, *Organic solar cell based on multistep charge separation system*, Applied Physics Letters (1992).

[18] Jen-Hsien Huang, Zhong-Yo Ho, Tsung-Hsien Kuo, Dhananjay Kekuda, Chih-Wei Chu, and Kuo-Chuan Ho, *Fabrication of multilayer organic solar cells through a stamping technique*, Journal of Materials Chemistry **19** (2009), no. 24, 4077.

[19] Jingsong Huang, Martin Pfeiffer, Ansgar Werner, Jan Blochwitz, Karl Leo, and Shiyong Liu, *Low-voltage organic electroluminescent devices using pin structures.*

[20] Jacek Jasieniak, Marco Califano, and Scott E. Watkins, *Size-dependent valence and conduction band-edge energies of semiconductor nanocrystals*, ACS Nano **5** (2011), no. 7, 5888–5902.

[21] Illan J Kramer, Gabriel Moreno-Bautista, James C Minor, Damir Kopilovic, and Edward H Sargent, *Colloidal quantum dot solar cells on curved and flexible substrates.*

[22] Kwan H Lee, Paul E Schwenn, Arthur RG Smith, Hamish Cavaye, Paul E Shaw, Michael James, Karsten B Krueger, Ian R Gentle, Paul Meredith, and Paul L Burn, *Morphology of all-solution-processed bilayer organic solar cells*, Advanced Materials **23** (2011), no. 6, 766–770.

[23] J Liu, J Liu, Y Shi, Y Shi, Y Yang, and Y Yang, *Solvation Induced Morphology Effects on the Performance of Polymer Based Photovoltaic Devices*, Adv. Funct. Mater. **11** (2001), no. 6, 420.

[24] Andrea Maurano, Rick Hamilton, Chris G. Shuttle, Amy M. Ballantyne, Jenny Nelson, Brian O'Regan, Weimin Zhang, Iain McCulloch, Hamed Azimi, Mauro Morana, Christoph J. Brabec, and James R. Durrant, *Recombination dynamics as a key determinant of open circuit voltage in organic bulk heterojunction solar cells: A comparison of four different donor polymers*, Advanced Materials **22** (2010), no. 44, 4987–4992.

[25] Jenny Nelson, James Kirkpatrick, and P. Ravirajan, *Factors limiting the efficiency of molecular photovoltaic devices*, Physical Review B **69** (2004), no. 3, 1–11.

[26] Wanyi Nie, Gautam Gupta, Brian K Crone, Feilong Liu, Darryl L Smith, P Paul Ruden, Cheng-yu Kuo, Hsinhan Tsai, Hsing-lin Wang, Hao Li, Sergei Tretiak, and Aditya D Mohite, *Interface Design Principles for High-Performance Organic Semiconductor Devices*, Advanced Science (2015), 1–7.

[27] Wanyi Nie, Hsinhan Tsai, Reza Asadpour, Amanda J Neukirch, Gautam Gupta, Jared J Crochet, Manish Chhowalla, Sergei Tretiak, Muhammad A Alam, and Hsing-lin Wang, *High-efficiency solution-processed perovskite solar cells with millimeter-scale grains* **347** (2015), no. 6221, 522–526.

[28] Ann G. Osborn and Donald R. Douslin, *Vapor pressure relations of 13 nitrogen compounds related to petroleum*, Journal of Chemical Engineering Data **13** (1968), no. 4, 534–537.

[29] Jack E Parmer, Alex C Mayer, Brian E Hardin, Shawn R Scully, Michael D Mcgehee, Martin Heeney, and Iain Mcculloch, *Organic bulk heterojunction solar cells using poly " 2,5-bis " 3-tetradecyllthiophen-2-yl... thieno 3,2,-b thiophene...*

[30] Mathew Peach, *Heliatek achieves* 12% *organic solar cell efficiency*, Optics.org (2013).

[31] William J Potscavage, William J Potscavage, Asha Sharma, Asha Sharma, Bernard Kippelen, and Bernard Kippelen, *Critical Interfaces in Organic Solar Cells and Their Influence on the Open-Circuit Voltage.*, Accounts of chemical research **xxx** (2009), no. xx.

[32] Hideki Shirakawa, J Louis, and Alan G Macdiarmid, *Synthesis of Electrically Conducting Organic Polymers : Halogene Derivatives of Polyacetylene, (CH)x*, J. C. S. Chem. Comm **578** (1977), 578–580.

[33] C. G. Shuttle, B. O'Regan, A. M. Ballantyne, J. Nelson, D. D C Bradley, and J. R. Durrant, *Bimolecular recombination losses in polythiophene: Fullerene solar cells*, Physical Review B - Condensed Matter and Materials Physics (2008).

[34] Henry J. Snaith, Neil C. Greenham, and Richard H. Friend, *The origin of collected charge and open-circuit voltage in blended polyfluorene photovoltaic devices*, Advanced Materials **16** (2004), no. 18, 1640–1645.

[35] Margaret A Stevens, *Employing Cascaded Energy Structures in Next-Generation Photovoltaic Devices by* (2014).

[36] Akira Tada, Yanfang Geng, Qingshuo Wei, Kazuhito Hashimoto, and Keisuke Tajima, *Tailoring organic heterojunction interfaces in bilayer polymer photovoltaic devices.*, Nature materials **10** (2011), no. 6, 450–455.

[37] C. W. Tang, *Two-layer organic photovoltaic cell*, Applied Physics Letters **48** (1986), no. 2, 183–185.

[38] The Mendeley Support Team, *Getting Started with Mendeley*, Mendeley Ltd., London, 2011.

[39] Bright Walker, Chunki Kim, and Thuc Quyen Nguyen, *Small molecule solution-processed bulk heterojunction solar cells*, Chemistry of Materials **23** (2011), no. 3, 470–482.

[40] Cordula D. Wessendorf, Regina Eigler, Siegfried Eigler, Jonas Hanisch, Andreas Hirsch, and Erik Ahlswede, *Investigation of pentaarylazafullerenes as acceptor systems for bulk-heterojunction organic solar cells*, Solar Energy Materials and Solar Cells **132** (2015), 450–454.

[41] M. Wiemer, M. Koch, U. Lemmer, a. B. Pevtsov, and S. D. Baranovskii, *Efficiency of exciton dissociation at internal organic interfaces beyond harmonic approximation*, Organic Electronics: physics, materials, applications **15** (2014), no. 10, 2461–2467.

[42] Keng Hoong Yim, Zijian Zheng, Ziqi Liang, Richard H. Friend, Wilhelm T S Huck, and Ji Seon Kim, *Efficient conjugated-polymer optoelectronic devices fabricated by thin-film transfer-printing technique*, Advanced Functional Materials **18** (2008), no. 7, 1012–1019.

[43] G. Yu, J. Gao, J. C. Hummelen, F. Wudl, and a. J. Heeger, *Polymer Photovoltaic Cells: Enhanced Efficiencies via a Network of Internal Donor-Acceptor Heterojunctions*, Science **270** (1995), no. 5243, 1789–1791.

[44] Wen Yuan, *Design and Development of Efficient Solid-State Dye-Sensitized Solar Cells* (2013).